



Fluid seepage associated with slope destabilization along the Zambezi margin (Mozambique)

Eric Deville, Carla Scalabrin, Gwenael Jouet, Antonio Cattaneo, Anne Battani, Sonia Noirez, Hélène Vermesse, Karine Olu, Laure Corbari, Marion Boulard, et al.

► To cite this version:

Eric Deville, Carla Scalabrin, Gwenael Jouet, Antonio Cattaneo, Anne Battani, et al.. Fluid seepage associated with slope destabilization along the Zambezi margin (Mozambique). *Marine Geology*, 2020, 428, pp.106275. 10.1016/j.margeo.2020.106275 . hal-03118579

HAL Id: hal-03118579

<https://ifp.hal.science/hal-03118579>

Submitted on 15 Jul 2022

HAL is a multi-disciplinary open access archive for the deposit and dissemination of scientific research documents, whether they are published or not. The documents may come from teaching and research institutions in France or abroad, or from public or private research centers.

L'archive ouverte pluridisciplinaire **HAL**, est destinée au dépôt et à la diffusion de documents scientifiques de niveau recherche, publiés ou non, émanant des établissements d'enseignement et de recherche français ou étrangers, des laboratoires publics ou privés.



Distributed under a Creative Commons Attribution - NonCommercial 4.0 International License

Fluid seepage associated with slope destabilization along the Zambezi Margin (Mozambique)

Eric Deville¹, Carla Scalabrin², Gwenael Jouet², Antonio Cattaneo², Anne Battani¹, Sonia Noirez¹, Hélène Vermesse¹, Karine Olu³, Laure Corbari⁴, Marion Boulard³, Tania Marsset², Massimo Dall'Asta⁵, Martina Torelli¹, Lucie Pastor³, Delphine Pierre², Benoit Loubrieu²

¹IFP-Energies Nouvelles, Rueil-Malmaison, France

²IFREMER, Géoscience Marines, Plouzané, France

³IFREMER, Unité Étude des Écosystèmes Profonds, Plouzané, France

⁴MNHN-UPMC, Paris, France

⁵TOTAL-CSTJF, Pau, France

ABSTRACT

Evidences for active fluid seepages have been discovered along the Zambezi continental slope (offshore Southern Mozambique). These seepages are mostly associated with pockmarks which are aligned along a trend parallel to the slope and running closely upstream of the headwall scarp of a wide zone of slope destabilization. Fluid seepages are interpreted as a potential trigger for the slope destabilization. Acoustic anomalies within the water column have been interpreted as related to moderate bubble seepages mostly located outside and only punctually inside the destabilization zone. Exploration with the SCAMPI towed camera system in the widest pockmark (diameter 200 m wide) has shown fluid seepages associated to authigenic carbonate crusts and bacterial mats. These fluid seepages are also associated to the presence of chemosynthetic organisms (Vesicomidae and Thyasiridae bivalves, Siboglinidae tubeworms). The sampled gas in the sediment corresponds mainly to CH₄ of microbial origin, generated by hydrogenotrophic methanogenesis from a substrate of organic origin, *i.e.* a conventional process of genesis of microbial gas in the marine domain. No evidence for thermogenic gas was detected. Another type of pockmarks has been observed within the core of the slope destabilization zone. Most of these pockmarks are inactive in terms of fluid seepage at present time and are associated to carbonate buildups forming chimney geometries. They probably correspond to diagenetic chimneys of former fluid migration pathways that have been exhumed during the mass sliding and the surrounding depression are related to recurrent activity of strong lateral slope currents which have scoured

the sediments around. The spatial organization of the slope destabilization features is considered as representative of the temporal evolution of the landslide giving information about the dynamics of slope instability processes. This proposed evolution started by scattered seepages of formation water with dissolved gas. Then free gas seepages appeared notably in the upper part of the slope. This was followed by progressive shallow deformation in the sediments downslope of the main gas seepages. Finally, the whole slope was destabilized forming imbricated landslides exhuming locally former diagenetic chimneys.

1. Introduction

Marine cold fluid seepages commonly develop along continental margins worldwide. Seepages are found from shallow to deep water domains and they are especially common in the external platform to the upper continental slope (King and MacLean, 1970; Deville et al., 2006; Gay et al., 2006; Judd and Hovland, 2007; Prinzhofer and Deville, 2013; Dupré et al., 2007, 2010, 2014, 2015; Mascle et al., 2014; Riboulot et al., 2018; Marsset et al., 2018). The widespread occurrence of fluid seepages along margins has been largely emphasized by increasing multibeam seabed coupled with water column studies during the last decades (Dupré et al., 2010, 2014). Fluid seepages are commonly associated with the precipitation of authigenic carbonates around the vents associated with the microbially driven oxidation of methane present within the fluid seepages by sea water sulfate (Naehr et al., 2000; Aloisi et al., 2002; Peckmann et al., 2001; Bayon et al., 2013; Rongemaille et al., 2011; Pierre et al., 2012, 2014, 2017). Fluid overpressure along continental slopes are commonly associated with sedimentary instabilities responsible for slope destabilization (Sultan et al., 2004a and b; Bunz et al., 2005; Urlaub et al., 2015; Elger et al., 2018). Reciprocally, slope destabilization is also locally a possible trigger for fluid seepage (Kramer et al., 2017). The present study focuses on fluid seepages and slope destabilization processes which have been observed along the Zambezi continental slope. It is based on the geophysical characterization of seep-related structures, water column acoustic anomalies, fluid emissions analysis and authigenic carbonate analysis. The objective of this paper is to better characterize these fluid seepages and to show how they are closely associated with a wide zone of destabilization of the sediments along the continental slope. The study area appears to correspond to a typical case where the spatial organization of the slope destabilization features seems directly

representative of the temporal evolution of the landslide providing information about the dynamics of slope instability processes.

2. Geological framework

The sediment accumulation on the Zambezi platform has occurred progressively during more than 140 Ma on the western continental margin of the Mozambique channel (Salman and Abdula, 1995; Walford et al., 2005) which developed since the breakup of Gondwana and the formation of the oceanic lithosphere of the Mozambique Channel during Jurassic times (Leinweber and Jokat, 2012; Reeves, 2014; Key et al., 2015; Mueller and Jokat, 2019; Thompson et al., 2019). The deep water area of the Mozambique basin is characterized by the development of an oceanic lithosphere which began to develop during the Mid Jurassic-Cretaceous drift of Antarctica with respect to Africa (Rabinowitz et al., 1983; Coffin and Rabinowitz, 1987). Nowadays, the central part of the Mozambique Channel is still tectonically active (Marsset et al., 2018; Deville et al., 2018) and presents an anomalously high topography (Castelino et al., 2016; Deville et al., 2018). The Zambezi River is the fourth main river of Africa in terms of water flux (after the Nile, the Congo and the Niger) and it is the main one along the east African coast. The solid particles transported by the Zambezi river have largely been deposited along the Zambezi platform which corresponds to a major accumulation of sediments (locally more than 6000 m) located along the east African transform passive margin, in the offshore of southern Mozambique (Walford et al., 2005; Mahajane, 2014; Ponte, 2018, 2019 and references therein) (Fig. 1). The oceanic domain of the Mozambique basin is also largely covered by sediments deriving from the Zambezi turbidite system (Kolla et al., 1980; Droz and Mougenot, 1987; De Ruijter et al., 2002; Walford et al., 2005; Kolla et al., 1991; Mahanjane, 2012; Mahanjane et al., 2014; Halo et al., 2014; Breitzke et al., 2017). The Zambezi river delivered more than 16×10^3 t/Ma of sediments during Quaternary times (Walford et al., 2005) but this flux has been disturbed recently by several dams trapping sediments in the Zambezi water shed (Moore et al., 2007). Nowadays, the Zambezi turbidite system is disconnected from the Zambezi river system (Schulz et al., 2011; Fierens et al., 2019; Miramontes et al., 2019). The sediments are dispersed by strong NNE-SSW trending coastal currents on the continental shelf (Schulz et al., 2011; Wiles et al., 2017a and b). A recent modeling approach suggested the activity of strong bottom current along the Zambezi continental slope mainly from NNE to SSW along

the Zambezi shelf (Mozambique current) and from SSW to NNE along the lower Zambezi slope (Mozambique undercurrent; Miramontes et al., 2019). The Zambezi margin is not affected by massive gravity shale tectonics processes like it is the case in similar shale-rich systems as the Niger Delta (Corredor et al., 2005), the Amazon (Cobbold et al., 2004) or the northern margin of Mozambique in the Rovuma basin (Mahanjane and Franke, 2014). One of the characteristics of the Zambezi platform and continental slope is that only the uppermost part of the sedimentary pile is affected by wide marine landslides which occurred repetitively (Ponte et al., 2018a and b). The sedimentary architecture of the Zambezi platform and continent slope correspond to a massive (> 2 km thick) prograding system from Early Miocen to present time (Ponte et al., 2018).

3. Material and methods

Geophysical acquisitions

The data presented in this study were acquired during PAMELA-MOZ04 (2015) survey on board the R/V *Pourquoi pas?* (Jouet and Deville, 2015) in the framework of the PAMELA research project (PAssive Margins Exploration LAboratories; Bourillet et al., 2013). Multibeam echosounder data were used for bathymetry mapping (Fig. 2) but also for the detection and location of free gas emissions in the water column through water depths ranging from 61 to 1021 m in the studied area (Fig. 3). The multibeam dataset was collected with a Reson Seabat 7111 for shallow waters (5 to 500 m, 100 kHz) and a Reson Seabat 7150 for deeper waters (200 to 4000 m, 24 kHz, across and along-track beam width of 0.5°). Beyond water depths of 500 m, the Reson 7150 (24 kHz) was used with the following configuration: multiping option (4 swaths per ping) with 880 beams and nominal swath coverage of 150° (effective average of 145°). The multibeam acoustic coverage was acquired at an average speed of 9 knots which allows an average inter-ping distance of 4.3 m. Also, 24-channel mini GI-gun seismic reflection data were acquired during the PAMELA-MOZ04 survey. In addition, hull mounted Sub-Bottom Profiler (SBP) was operated in a chirp configuration (1.8-5.2 kHz) that offers a vertical resolution of 0.30 m and a maximal penetration of 100 m.

SCAMPI system

The SCAMPI (Système de CAMéras Ponctuel Interactif) is a towed system devoted to make direct observations at the sea bottom and to acquire submarine photos and video shooting. It is designed to operate between 3 and 10 m above the seabed and down to 6000 m of water depth. A CTD sensor was also mounted on the frame, monitoring water depth and temperature along the SCAMPI track. In the study area, it was operated during two dives (SCB01 and SCB03) on two different areas where pockmarks are present (Fig. 2).

Gas sampling and geochemical study

Gas was sampled in three Calypso sediment piston cores (MOZ04-CS18 and MOZ04-CS19, and also MOZ04-CS17 made north of the study area; see supplementary material Fig. S1, S2, S3). The gas samples were collected using two different procedures: either directly as free gas that degassed from the sediment in the liner of core MOZ4-CSF19, or in the form of adsorbed gas in the sediment collected at the bottom of the cores MOZ4-CS17, MOZ4-CSF18 and MOZ4-CSF19. The free gas was sampled from the holes made in the PVC liners at the base of the piston cores to fix the corer bits. The sediments collected at the bottom of the cores, in the corer bits (*i.e.* at the deepest part of the cores), were placed in 200 ml glass bottles in order to recover the adsorbed gas in the sediment. The samples were conditioned with a 10 ml air head-space, 90 ml of sediment and 90 ml of water with 10 drops of mercury dichloride (HgCl_2 ~ 1/1000) in order to stop microbial activity after sampling. Samples were stored at 4°C. The gas was recovered in 10 ml Labco vials using a double needle for analysis.

The chemical compositions of the gases were determined by gas chromatography (GC). The $^{13}\text{C}/^{12}\text{C}$ isotopic ratio measurements (CH_4 and CO_2) were determined on a MAT253 (Thermo Fischer) mass spectrometer coupled to a gas chromatograph (GC-C-IRMS for Gas Chromatography Combustion Isotope Ratio Mass Spectrometry). Detailed procedure is available in Appendix 2 in supplementary material.

Carbonate sampling and geochemical study

Carbonate concretions have been recovered with multitube sampler inside the main pockmark where MOZ04-MTB5 has been cored (Fig. 4). Attempts to recover carbonates with a Warren dredge were not successful. The mineralogy and the respective contents of the different carbonates have been determined by rock-eval method (Pillot et al., 2015). Isotopic

measurements were made on the bulk rock powder using a standard continuous flow Isotope Ratio Mass Spectrometry at the Erlangen University.

4. Results

Morphobathymetric features

Geophysical data have shown that the area studied, running parallel to the continental shelf trend from SW to NE, corresponds to a portion of the Zambezi margin covering parts from the shelf-break of the Zambezi platform to deep water areas along the Zambezi slope (down to -1200 m; Fig. 2). This area shows a NE-SW segmentation of the geomorphological features. The NE area corresponds to a sedimentary slope dipping towards the South-East which is preserved from any gravitational destabilization. The southwest area shows a more complex pattern and the slope exhibits massive evidences of gravitational destabilization made of imbricated mass-transport complexes with coarse outrunner blocks downslope (Fig. 2). The destabilized area is localized south of the Zambezi River mouth. The thickness of the destabilized sediments varies from less than 25 m to more than 150 m (Fig. S5 and S6 in supplementary material). The topography of the destabilized zone exhibit some gullies trending dip-slope with smooth morphology (Fig. 2). Globally, from the NE to the SW, the slope shows a progressive evolution from (1) a stable area to (2) an area of moderate destabilization characterized by progressive deformation of the slope, to finally (3) imbricated and polyphase system of landslides toward the southwest. Each individual landslide unit forms elongated tongue along the slope for which the detachment level varies from one tongue to another. In the different domains from the stable area to the massive destabilization area, different types of pockmarks with distinctive characteristics have been discovered, providing evidences for active or fossil fluid seepage.

Pockmarks outside the destabilization zone

The pockmarks identified on geophysical data which are located outside of the destabilization zone are shown in Figs. 2, 4 and 5. Some of these pockmarks are located northeast and partly upstream of the northeast extremity of the zone of slope destabilization. A relatively well organized alignment exists between the pockmarks located to the northeast of the slope destabilization zone and the pockmarks located immediately upstream of the scarp of the

upper part of the SW slide area (Fig. 2). Several pockmarks are associated with acoustic anomalies in the water column (Fig. 3). The morphology of these anomalies, as observed with a RESON 7150 MBES, is characteristic of free gas emissions in the water column and their weak backscattering amplitude may indicate a low flow of bubbles (Fig. 3).

Northeast of the destabilization zone, the multibeam data acquired allowed us to identify several tens of pockmarks. The main ones are mapped in figure 2 and SBP profiles crossing them are presented in figures 4 and 7. During the SCAMPI dive MOZ04-SCB03, observations at the sea bottom have been made within and around the largest pockmark which corresponds to an isolated depression of 200 m in diameter located at 300 m of water depth (Fig. 4). Sampling with a multitube core system (MOZ04-MTB5) was made inside this pockmark, and a Calypso piston core (MOZ04-CSF19) was recovered 150 m south of this pockmark. The center of this pockmark is characterized by a more reflective character on the SBP data (see supplementary material; Fig. S4). The multitube coring (MOZ04-MTB5) made in the center of this structure collected sandy sediments with carbonate concretions (Figs. 5, 6). The MOZ04-CSF19 Calypso core shows sandy levels in the upper 2 meters and clay-rich sediments below (supplementary material Fig. S1). When it returned on deck, the base of the core was degassing and free gas was directly flowing out from the liner of the core. The SCAMPI dive (MOZ04-SCB03: Figs. 4, 5) carried out in this pockmark area has shown a moderate activity of fluid seepages (water) without apparent free gas bubbling. In the center of the structure, we observed several active vents piercing the sandy surface of the seafloor. These vents were characterized by the presence of reduced gray/blue sediments and white areas (mineral precipitation and/or bacterial mats). Carbonate concretions (of maximum metric horizontal size) have also been observed (Fig. 5). Episodic turbid flows emerging from these vents have been punctually observed on video shooting (Fig. 5, arrows). The temperature of the water near the bottom during the SCAMPI dive MOZ04-SCB03 in the seepage area, where the carbonate samples were collected, was relatively constant between 12.07 and 12.21°C (no obvious thermal anomaly). No acoustic anomalies in the water column were observed along the profiles acquired over this pockmark. This is probably due to the fact that no free gas bubble is expelled from this pockmark. The peripheral zone of the pockmark is mainly populated by Cnidarians (Pennatulids). Their density is low but increases towards the border of the pockmark. They are associated to ripple marks related to bottom current that suspend organic matter issued the pockmark area. OM is then used by these suspension-feeders organisms. Low densities of mollusks (Buccinidae and Ranellidae gastropods),

crustaceans (Inachidae), echinoderms (crinoids, asterids) were also observed in this peripheral zone of the pockmark.

At the border of the pockmark depression, the Pennatula density increases and in the center of the depression, a lobster colony (*Palinurus delagoae*) was observed. The presence of bivalve shells belonging to the families Vesicomidae and Thyasiridae is also abundant. These bivalves are common in methane seepage area as they host in their gills symbiotic bacteria whose metabolism is based on chemiosynthesis (sulfide oxidation) (Dubilier et al., 2008; Duperron et al., 2013). Also, bouquets of polychaete tubeworms belonging to the family Siboglinidae (vestimentiferans) were observed. These tubicolous worms are also common in methane seepage area as they have also the particularity of living in symbiosis with chemio-autotrophic bacteria, which use sulphides produced in the sediments (Dubilier et al., 2008). Hydrogen sulphide is produced by anaerobic methane oxidation coupled to sulfate reduction at cold seeps (Boetius et al., 2000). The pockmark visited during the MOZ04-SCB03 SCAMPI dive is among the wider of the NE part of the study area but other similar structures are also present in this area (Fig. 2). They are also associated with characteristic subvertical seismic anomalies seen in SBP data (see examples in Fig. 7A and B). Note also that clear and localized reflectivity anomalies are probably related to the presence of free gas as they are present only locally in thin antiform layers of the uppermost sediments of this area and they are not related to characteristic sedimentary structures which might be responsible for the reflectivity anomalies (Fig. 7C).

Pockmarks inside the destabilization zone

Different types of pockmarks have been found inside the destabilization zone. Some of them are located in the northeast most area of the destabilized area. They have a relatively small size (lower than 200 m), they have elongated shapes and they correspond shallow deformation structures possibly associated to a dewatering process during the slope deformation (Figs. 2; S5). Locally, inside the destabilized zone, some moderate positive reliefs are associated with acoustic anomalies in the water column above (see supplementary material; Fig. S6). They possibly correspond to moderate gas bubbling associated with the precipitation of carbonate buildups or mud volcanoes. The pockmarks which are located in the center of the destabilized zone immediately below the main landslide headwall scarp (Fig. 2, 8, 9, 10, 11) are more than 200. Only the main ones are plotted on figure 2. Their size does not exceed 50 m in diameter. The location of these pockmarks in the center of the landslide area strongly suggests a

potential link between them and the origin of the slope destabilization process. The most characteristic pockmarks inside the slope destabilization zone are formed by comet-shaped depressions (Fig. 11). Despite of their small size, on multibeam data, it is possible to distinguish small positive reliefs in the center of some of these structures (Fig. 11). The center of these pockmarks also presents high reflectivity on sub-bottom profiler data (see supplementary material, Fig. S7). During the SCAMPI MOZ04-SCB01 dive in the area, carbonate buildups have been observed in the center of the pockmarks with circular depressions around (Fig. 11). Some carbonate buildups present pipes geometries. The most characteristic have cylindrical shapes with vertical sides and are 3 to 4 m in diameter at their base, for a height of up to about 8 m. No evidence for active fluid flows at these chimneys was observed during the dive neither in the water column above. Calypso coring CSF18 sampled dark clay-rich homogeneous sediments without sedimentary structures (see supplementary material; Fig. S2). The sediments sampled in this core correspond to an Holocene cover deposited in the bottom of the depression formed during the slide. A Warren dredging collected also mainly dark mud in which were present many dead organisms but it was not possible to collect any of the carbonate material seen during the SCAMPI dive.

The density of pockmarks with chimney inside is higher near the scarp and decreases downslope towards the southeast. Some groups of these pockmarks are aligned according to a dip-slope direction (Figs. 9, 10). These pockmark alignments in the direction of the slope suggest a subsurface control of the orientation of these lineaments by NW-SE buried structures (possibly buried channels or canyons, or faults). Down along the slope (below 600 m of water depth), blocks are visible on multibeam data (Fig. 9). These translated blocks are probably mainly made of carbonates issued from the platform (the main outcropping solid rocks along the Zambezi margin) and so they are regarded as having a different origin than the chimneys located upslope (mainly above - 600 m; Fig. 9).

Acoustic anomalies in the water column are associated with some of these pockmarks. The anomalies correspond to sub-horizontal diffusive layers on sonar data (see supplementary material; Fig. S8) which are elongated downstream, *i.e.* in the direction of the bottom current flowing SE (the direction of strong bottom current has been directly observed during the towing of the SCAMPI). These acoustic anomalies initiated at pockmarks with carbonate inside correspond probably to flows of particles issued from the pockmarks and carried by the bottom current toward the southeast. Some of these pockmarks are comet tail-shaped, pointing towards the southeast, which is in good agreement with erosion related to this direction of downslope current. The trend of several gullies is also compatible with erosion

associated with this downslope current (Figs. 8, 9). The calypso coring (CSF18) made in the area of this pockmark cluster did not reveal any particular evidence that could be associated with active fluid flows (supplementary material Fig. S2).

Gas study

Since the gas sampling was done on coring equipment which was largely in contact with the atmosphere during the recovery of the cores onboard, a significant proportion of air contributed, in all cases, to dilute the initial gas composition (Tables 1 and 2). The chemical composition of the gas which was degassing from the core MOZ4-CSF19 made close the active pockmark of the SCAMPI dive MOZ04-SCB03 (*i.e.* where fluid seepage have been observed) shows mainly methane and for a minor part CO₂ with traces of C₂ + (contents less than 0.01%). The isotopic composition of the methane collected in the core MOZ4-CSF19 shows $\delta^{13}\text{C-CH}_4$ values of -92.2‰ for the free gas seeping out from the liner of the core and -86.7‰ for the gas adsorbed in the sediments of the corer bit, at the most bottom of the core (Fig. 12; table 2) and $\delta\text{D-CH}_4$ from -182.2‰ for the free gas to -170.5‰ in the sediments of the corer bit (Fig. 13; table 2). The isotopic composition of the CO₂ collected in the core MOZ4-CSF19 shows values of $\delta^{13}\text{C-CO}_2$ of -44.5‰ for the free gas and -23.8‰ at the lowest part of the core (Fig. 14; table 2). No important degassing was observed in cores MOZ4-CSF17 an MOZ4-CSF18, only adsorbed gas was sampled. Geochemical signatures of these gas samples are very similar to those of core MOZ4-CSF19 (Figs. 12, 13, 14).

Authigenic carbonates

Carbonates in the fluid conduits, which have been recovered with multitube sampler inside the main pockmark of the preserved northern area (MOZ04-MTB5), are made of calcite and aragonite (RE6 determination; see supplementary material Fig. S9). Isotopic composition of these carbonates show $\delta^{18}\text{O}$ bulk rock values ranging between 2.89 and 3.47‰ vPDB and $\delta^{13}\text{C}$ bulk rock values between -48.87 and -52.50‰ vPDB (Fig. 15, table 3).

5. Discussion

Pockmark activity

North-east of the slope destabilization zone a system of pockmarks has been characterized forming (1) depressions aligned NE-SW between 200 and 300 m of water depth and (2) scattered depressions in the slope below 300 m of water depth (Fig. 2). Active fluid seepage corresponding to water escape has been characterized by direct observation thanks to the SCAMPI in the wider pockmark in the NE of the study area. Acoustic anomalies in the water column corresponding most probably to free gas bubbles seepages have been characterized close to the northeast border of the landslide area and upslope of the landslide area. Inside the landslide, active seepages are rare except punctual seepages but most of the pockmarks are inactive today. These depressions do not show typical characters of active fluids seepages at the seabed. It is probable that to the center of these depressions is the place of fossil deep diagenetic chimneys exhumed during the sliding. They probably correspond to former fluid migration pathways. These chimneys have probably been active partly after the landslide because they appear inside the Holocene sedimentary cover that is preserved at the center of the landslide area (Fig. 10C) but they are inactive today. They would then correspond to exhumed ancient fluid chimneys similar for instance to those described onshore in Bulgaria by De Boever et al. (2006). The peripheral depression of the chimneys could be recent and linked to the action of the currents which scour the sediment around the rigid chimneys. This would explain the turbidity of the water observed during the SCAMPI dive (MOZ04-SCB01) and the diffusive layer detected by multibeam acquisition in the water column (see supplementary material; Fig. S8). The fluids which have circulated in these ancient chimneys could have been at the origin of overpressures which initiated the gravitational mass movements (Sultan et al., 2004a and b; Bull et al., 2009). Overpressure are prone to develop at relatively shallow depths (few tens of meters) taking into account the low permeability of the sediments and the high sedimentation rate along the Zambezi platform and slope. A seismic reflection profile acquired upstream of the landslide area provides an image of what could have been the initial geometry before the slide (Fig. 10A). The landslide tends to be sealed by the Holocene sediments and it was possibly active mainly during lower stand of sea level. Indeed, the conjunction of overpressure in the sediments with decreasing load above (associated in this case with a drop of sea level) is classically considered as favorable to reach failure condition and so to initiate landslide (Hubbert and Rubey, 1959, Byerlee, 1978).

Origin of fluids

Geochemical analyses have shown that the gas has a typical microbial origin mainly generated according to a CO₂ reduction pathway from a substrate of organic origin (Fig. 12, 13, 14), *i.e.* a conventional microbial gas genesis process in the marine domain (Whiticar, 1999). No isotopic evidence for thermogenic gas was detected. The $\delta^{13}\text{C-CO}_2$ values are indicative of the degradation of an organic source consisting of solid organic matter rather than liquid hydrocarbons (in this case the $\delta^{13}\text{C-CO}_2$ are generally $> -10\text{‰}$; Milkov and Etiope, 2018). CH₄ is the dominant gas in both the free gas and the adsorbed/dissolved gas in sediment porewater. Note that the fauna composition observed during the MOZ04-SCB03 SCAMPI dive is in good concordance with the presence of fluid seepage associated with dissolved methane. Differences are noticeable between the free gas taken from the liners and the gas adsorbed in the sediments of the base of the core and recovered in head-spaces. Indeed, there is a difference of about $+20\text{‰}$ $\delta^{13}\text{C-CO}_2$ and $+5\text{‰}$ $\delta^{13}\text{C-CH}_4$ between, respectively, the free gas and the gas recovered in the head-spaces of the corer bits (Fig. 14; full arrows). The fact that methane $\delta^{13}\text{C}$ shows low values in offshore Mozambique suggests that the organic substrate of the methane source is composed of isotopically light carbon (probably very rich in moist forest C3 plants, O'Leary, 1988). Values of $\delta^{13}\text{C-CO}_2$ are between -23.8 and -44.5‰ . The ^{13}C depletion of CH₄ is also linked to a decrease in the CH₄/CO₂ ratio and the ^{13}C depletion of CO₂ is accompanied by an increase in the CH₄/CO₂ ratio (Table 2). Similar characteristics have been previously interpreted either as microbial production of very light methane immediately below the Sulfate-Methane Transition Zone (SMTZ) (Whiticar, 1999), or as related to a moderate anaerobic oxidation process of the methane in the zone of very low sulfate concentration below the SMTZ and a light methane back-production process under the SMTZ (thermodynamic process, Yoshinaga et al., 2014). Indeed, the reactions catalyzed by enzymes being reversible, with the approach of thermodynamic equilibrium, in the zone with low concentration of sulfates, an inverse reaction to the Anaerobic Oxidation Methane (AOM) is probable therefore with reduction of dissolved CO₂ and production of methane (Yoshinaga et al., 2014). The isotopic carbon separation values between CH₄ and CO₂ ($\Delta\text{C}_{\text{CH}_4\text{-CO}_2}$), are between 62.9 and 47.7 in the core MOZ4-CSF19 in the Zambezi offshore which is a classical fractionation value for microbial gas related to biogenic CO₂ reduction in marine sediments (Whiticar, 1999). The isotopic analysis of the authigenic carbonates inside the sampled pockmark have shown very low $\delta^{13}\text{C}$ values (Fig. 15), which are very typical of microbial methane derived carbonate precipitations (Aloisi et al., 2002; Peckmann et al., 2001; Peckman and Thiel, 2004; Bayon et

al., 2013; Pierre et al., 2017). In cold seep environments, authigenic carbonate formation is driven by the activity of microbial consortium of sulfate-reducing bacteria and methanotrophic archaea (Boetius et al., 2000; Orphan et al., 2001). A mixture of fluids between organic matter and DIC of seawater is not suitable to explain the very enriched in ^{12}C compositions (marine carbonates which are not derived from microbial methane oxidation have $\delta^{13}\text{C}$ value commonly higher than -30‰). It is necessary to invoke another source of carbon with low $\delta^{13}\text{C}$ values to explain these isotopic compositions of the carbonates. In the near subsurface below the sea bottom, sulfate is prone to be reduced to sulphide while anaerobic oxidation of methane produces dissolved CO_2 in the SMTZ. The related increase of DIC concentration is prone to react with Ca^{2+} (and Mg^{2+}) of sea water in the uppermost sediments (in the oxic zone) generating carbonates. Thus, microbial methane as the source of carbon can explain the isotopic compositions of the carbonates discovered within the pockmark where the MOZ04-MTB5 was cored. Indeed, in this site, methane is extremely rich in ^{12}C ($\delta^{13}\text{C}\text{-CH}_4$ between -92.2‰ and -86.7‰ ; see above) as it is the case for the carbonates. The isotopic fractionation between CO_2 and calcite precipitation ($\Delta\text{C}_{\text{CO}_2\text{-calcite}}$) at 12°C is equal to -10‰ (Emrich et al., 1970). This is consistent with the value measured here which is $\Delta\text{C}_{\text{CO}_2\text{-calcite}} = -8.1$. Thus, the isotopic compositions of the gas and of the carbonates are both consistent with a microbial origin of the gas seepages.

Fluid seepages and slope destabilization

The study of the distribution of fluid seepages (active and fossil) in the Zambezi slope suggests a strong interaction between fluid dynamics and gravitational slope destabilization. Active pockmarks are seen mostly outside of the destabilized zone. The pockmarks are scattered in the northeast of the study area (stable slope area). Close to the destabilized area, they tend to form an alignment trending parallel to the upslope boundary of the landslide area. Within this alignment, acoustic anomalies in the water column, which are probably related to bubble flows, appear close to the landslide area (northeast and upslope of the landslide; Fig. 2, 3). The pockmarks visible in the center of the destabilized zone correspond mainly to carbonated chimneys interpreted as ancient fluid conduits which are inactive today. The spatial evolution of the structure of the study area, from the northeast to the southwest, seems directly representative of the temporal evolution of the progressive fluid-landslide interaction processes (Fig. 16). Following this interpretation, stage 1 corresponds to a situation of stable

slope only pierced by scattered moderate cold fluid seepages of formation water with dissolved microbial methane. This seepage generates pockmark depressions paved by authigenic carbonates close and at the sea bottom. Stage 2 corresponds to a situation of higher density of fluid seepages, some of them being related to free gas bubbling. At this stage, an alignment of active pockmarks is formed in the upper part of the slope. This alignment is probably related to the development of an open fracture system at the initial stage of the destabilization process which has evolved at stage 3 as the headwall scarp of the landslide. Stage 3 corresponds to a moderate gravitational mass movement of the upmost sediment associated locally with free gas fluxes. At this stage, the headwall scarp of the landslide is initiated immediately downslope of active pockmark trend and below a zone of deformed sediments is formed, possibly related to a progressive gravitational creeping. The fact that gas seepages develop first and that only after landslide and headwall scarp fault appear suggests that the fluids are the trigger to the landslide and, in this case, the seepage cannot be considered as a simple consequence of the landslide. We interpret the fluid seepages as a consequence of overpressure at depth, high enough to breach the seal rocks. Finally, stage 4 corresponds to a situation of massive destabilization of the slope, with polyphased and imbricated mass-transport complexes involving deeper decollement levels compared to stage 3. This process is responsible for the exhumation of the pre-existing fluid conduits. At this stage fluid seepages tend to be not active anymore.

Conclusion

Active fluid seepages which have been discovered along the Zambezi continental slope correspond to water flows with dissolved methane in the stable parts of the slope and they tend to form water and free gas seepages trending parallel to the slope and running upslope of the headwall scarp of a wide zone of slope destabilization. Geochemical analyses indicates a microbial origin of the gas and this interpretation is supported by the geochemistry of associated authigenic carbonates. In the center of the zone of massive slope destabilization, no active seepages have been characterized. The fluid seepages have been interpreted as a consequence of fluid overpressure related to the huge accumulation of sediments below the Zambezi platform and the continental slope. Overpressure has been interpreted as the potential trigger for fluid migration and slope destabilization. The spatial organization of the slope destabilization features appears as representative of the temporal evolution of the

landslide history giving information about the dynamics of slope instability processes. Following this interpretation, it is suggested that it is the fluid dynamics including free gas seepage which occurred first before the progressive destabilization of the slope.

Acknowledgements

This work has been conducted within the framework of the PAMELA (PAssive Margin Exploration Laboratories) project leaded by IFREMER and TOTAL in collaboration with IFP Energies nouvelles, Université de Bretagne Occidentale, Université de Rennes 1, Sorbonne Université and CNRS. Data acquisition was made in 2015 during the PAMELA-MOZ04 survey (Jouet and Deville, 2015) onboard the R/V *Pourquoi Pas?* We thank captains, officers, crew members and the scientific team of the PAMELA-MOZ4 cruise for their technical support in recovering dataset.

References

- Aloisi, G., Bouloubassi, I., Heijs, S.K., Pancost, R.D., Pierre, C., Damste, J.S.S., Gottschal, J.C., Forney, L.J., Rouchy, J.M., 2002. CH₄-consuming microorganisms and the formation of carbonate crusts at cold seeps. *Earth Planet. Sci. Lett.* 203, 195–203. [http://dx.doi.org/10.1016/s0012-821x\(02\)00878-6](http://dx.doi.org/10.1016/s0012-821x(02)00878-6)
- Aloisi, G., Pierre, C., Rouchy, J.M., Faugeres, J.C., 2002. Isotopic evidence of methane-related diagenesis in the mud volcanic sediments of the Barbados Accretionary Prism. *Cont. Shelf Res.* 22, 2355–2372. [http://dx.doi.org/10.1016/s0278-4343\(02\)00061-4](http://dx.doi.org/10.1016/s0278-4343(02)00061-4)
- Bayon, G., Dupré S., Ponzevera, E., Etoubleau, J., Chéron, S., Pierre, C., Mascle, J., Boetius, A., de Lange G., 2013. Formation of carbonate chimneys in the Mediterranean Sea linked to deep-water oxygen depletion. *Nature Geoscience* 6, 755-760.
- Boetius, A., Ravensschlag, K., Schubert, G.J., Rickert, D., Widdel, F., Gieseke, A., Amann, R., Jorgensen, B.B., Witte, U., Pfannkuche, O., 2000. A marine microbial consortium apparently mediating anaerobic oxidation of methane. *Nature* 407, 623-626.
- Bourillet, J.F., Ferry, J.N., Bourges, P., 2013. PAMELA, Passive Margins Exploration Laboratories. <http://dx.doi.org/10.18142/236>

- 499 Braun, J, Guillocheau, F, Robin, C, Baby, G, Jelsma, H., 2014. Rapid erosion of the Southern
500 African Plateau as it climbs over a mantle superswell. *Journal of Geophysical Research*,
501 American Geophysical Union, 119 (7), 6093-6112. <https://doi10.1002/2014JB010998>.
- 502 Breitzke, M., Wiles, E., Krockner, R., Watkeys, M.K., Jokat, W., 2017. Seafloor morphology
503 in the Mozambique Channel: evidence for long-term persistent bottom-current flow and
504 deep reaching eddy activity. *Marine Geophysical Research* 38, 241–269.
505 <https://doi10.1007/s11001-017-9322-7>.
- 506 Bull, S., Cartwright, J., Huuse, M., 2009. A review of kinematic indicators from mass-
507 transport complexes using 3D seismic data. *Marine and Petroleum Geology* 26, 7, 1132-
508 1151. <https://doi.org/10.1016/j.marpetgeo.2008.09.011>.
- 509 Bünz, S., Mienert, J., Bryn, P. & Berg, K., 2005. Fluid flow impact on slope failure from 3D
510 seismic data: a case study in the Storegga Slide. *Basin Research* 17, 109–122.
511 <https://doi.org/10.1111/j.1365-2117.2005.00256.x>
- 512 Byerlee, J.D., 1978. Friction of rocks. *Pure Appl. Geophys.*, 116: 615-626.
- 513 Cobbold, P.R., Mourgues, K., Boyd, K. 2004. Mechanism of thin-skinned detachment in the
514 Amazon Fan: assessing the importance of fluid overpressure and hydrocarbon generation.
515 *Marine and Petroleum Geology*, 21, 1013–1025.
- 516 Castelino, J.A., Eagles, G., Jokat, W., 2016. Anomalous bathymetry and palaeobathymetric
517 models of the Mozambique Basin and Riiser Larsen Sea. *Earth and Planetary Science*
518 *Letters* 455, 25-37. <https://doi.org/10.1016/j.epsl.2016.09.018>
- 519 Coffin, M. F., Rabinowitz, P.D., 1987. Reconstruction of Madagascar and Africa: Evidence
520 from the Davie Fracture Zone and Western Somali Basin, *J. Geophys. Res.*, 92(B9), 9385–
521 9406, <https://doi:10.1029/JB092iB09p09385>
- 522 Corredor, F., Shaw, J.H., Bilotti, F., 2005. Structural styles in the deep-water fold and thrust
523 belts of the Niger Delta. *AAPG Bull.* 89 (6), 753–780.
- 524 De Boever, E, Swennen, R, Dimitrov, L, 2006. Lower Eocene carbonate cemented chimneys
525 (Varna, NE Bulgaria): Formation mechanisms and the (a)biological mediation of chimney
526 growth? *Sedimentary Geology*. <https://doi:10.1016/j.sedgeo.2005.12.010>
- 527 De Ruijter, W.P.M., Ridderinkhof, H., Lutjeharms, J.R.E., Schouten, M.W., Veth, C., 2002.
528 Observations of the flow in the Mozambique Channel: observations in the Mozambique
529 channel. *Geophysical Research Letters* 29, 140-1-140–3. 824
530 <https://doi.org/10.1029/2001GL013714>
- 531 Deville, É., Guerlais, S-H., Callec, Y., Griboulard, R., Huyghe, P., Lallemand, S, Mascle, A.,
532 Noble, M., Schmitz, J. and the CARAMBA research team, 2006. Liquefied vs Stratified

- Sedimentation Mobilization Processes: Insight from the South of the Barbados
Accretionary Prism. *Tectonophysics*, 428, 33-47. <https://DOI:10.1016/j.tecto.2006.08.011>
- Deville, E., Marsset, T., Courgeon, S., Jatiault, R; Ponte, J.P., Thereau, E., Jouet, G., Jorry, S.,
Droz, L., 2018. 826. Active fault system across the oceanic lithosphere of the Mozambique
Channel: Implications for the Nubia-Somalia southern plate boundary. *Earth and Planetary
Science Letters* 502, 210-220. <https://doi.org/10.1016/j.epsl.2018.08.052>
- Droz, L., Mougénot, D., 1987. Mozambique upper fan: origin of depositional units. *AAPG
Bulletin* 71, 838 1355–1365.
- Dubilier, N., Bergin, C., Lott, C., 2008. Symbiotic diversity in marine animals: the art of
harnessing chemosynthesis. *Nat. Rev. Microbiol.* 6, 725-740.
<https://doi:10.1038/nrmicro1992>
- Duperron, S., Gaudron, S.M., Rodrigues, C.F., Cunha, M.R., Decker, C., Olu, K., 2013. An
overview of chemosynthetic symbioses in bivalves from the North Atlantic and
Mediterranean Sea. *Biogeosciences* 10, 3241-3267. <https://doi.org/10.5194/bg-10-3241-2013>
- Dupré, S., Woodside, J., Foucher, J.-P., deLange, G., Mascle, J., Boetius, A., Mastalerz, V.,
Stadnitskaia, A., Ondréas, H., Huguen, C., Harmegnies, F., Gontharet, S., Loncke, L.,
Deville, E., Niemann, H., Omeregic, E., Olu-LeRoy, K., Fiala-Medioni, A., Dähl- mann,
A., Caprais, J.-C., Prinzhofer, A., Sibuet, M., Pierre, C., Sinninghe Damsté, J., NAUTINIL
scientific Party, 2007. Seafloor geological studies above active gas chimneys off Egypt
(Central Nile Deep Sea Fan). *Deep Sea Research Part I: Oceanographic Research Papers*,
vol.54, 1146–1172. <https://doi:10.1016/j.dsr.2007.03.007>
- Dupré, S., Woodside, J., Klauke, I., Mascle, J., Foucher, J.-P., 2010. Widespread active
seepage activity on the Nile Deep Sea Fan (offshore Egypt) revealed by high-definition
geophysical imagery. *Marine Geology* 275, 1–19.
- Dupré, S., Mascle, J., Foucher, J.-P., Harmegnies, F., Woodside, J., Pierre, C., 2014. Warm
brine lakes in craters of active mud volcanoes, Menes caldera off NW Egypt: evidence for
deep-rooted thermogenic processes. *Geo-Marine Letters* 34, 153–168.
<http://dx.doi.org/10.1007/s00367-014-0367-1>.
- Dupré, S., Scalabrin, C., Grall, C., Augustin, J.M., Henry, P., Celal Şengör, A.M., Görür, N.,
Namık Çağatay, M., Géli, L., 2015. Tectonic and sedimentary controls on widespread gas
emissions in the Sea of Marmara: Results from systematic, shipborne multibeam
echosounder water column imaging. *Journal of Geophysical Research: Solid Earth*
- Fierens, R., Droz, L., Toucanne, S., Raison, F., Jouet, G., Babonneau, N., Miramontes, E.,
Landurain, S., Jorry, S., 2019. Late Quaternary geomorphology and sedimentary processes

- in the Zambezi turbidite system (Mozambique Channel). *Geomorphology*
<http://doi.org/10.1016/j.geomorph.2019.02.033>
- Gay, A., Lopez, M., Cochonat, P., Séranne, M., Levaché, D., Sermondadaz, G., 2006. Isolated seafloor pockmarks linked to BSRs, fluid chimneys, polygonal faults and stacked Oligocene-Miocene turbiditic palaeochannels in the Lower Congo Basin. *Marine Geology* 226, 25-40.
- Halo, I., Backeberg, B., Penven, P., Ansorge, I., Reason, C., Ullgren, J.E., 2014. Eddy properties in the Mozambique Channel: A comparison between observations and two numerical ocean circulation 52 866 models. *Deep Sea Research Part II: Topical Studies in Oceanography* 100, 38–53. <https://doi.org/10.1016/j.dsr2.2013.10.015>
- Jouet, G., Deville, E., 2015. PAMELA-MOZ04 cruise, RV Pourquoi-Pas ?, <http://dx.doi.org/10.17600/15000700>
- Judd, A.G., Hovland, M., 2007. Seabed Fluid Flow: The Impact on Geology, Biology and Marine Environment. Cambridge University Press, New York, 475 pp.
- Elger, J., Berndt, C., Rüpke, L., Krastel, S., Gross, F., Geissler, W.G., 2018. Submarine slope failures due to pipe structure formation. *Nature Communications*, 9, 715. <https://doi.org/10.1038/s41467-018-03176-1>
- Frey-Martinez, J., Bertoni, C., Gerard, J., Matias, H., 2011. Processes of submarine slope failure and fluid migration on the Ebro continental margin: Implications for offshore exploration and development. Mass-transport deposits in deepwater settings, SEPM Special Publication n°96, Craig Shipp et al. (eds), ISBN 978-1-56576-287-9, 181-198.
- Gee, M.R., Uy, H.S., Warren, J., Morley, C.K., Ferguson, A., Lauti, S., Lambiase, J.J., 2007. The Brunei Slide: a giant submarine landslide on the North West Borneo Margin revealed by 3D seismic data. *Mar. Geol.* 246, 2-9. <http://dx.doi.org/10.1016/j.margeo.2007.07.009>.
- Horozal, S., Bahk, J.J., Urgeles, R. , Young Kim, G. , Cukur, D., Kim, S.P. , Hoon Lee, G., Hoon Lee, S., Ryu, B.-J., Kim, J.-H., 2017. Mapping gas hydrate and fluid flow indicators and modeling gas hydrate stability zone (GHSZ) in the Ulleung Basin, East (Japan) Sea: Potential linkage between the occurrence of mass failures and gas hydrate dissociation. *Marine and Petroleum Geology* 80, 171-191, <https://doi.org/10.1016/j.marpetgeo.2016.12.001>.
- Hubbert, M.K., Rubey, W.W., 1959. Role of fluid pressure in mechanics of overthrust faulting: I. Mechanics of fluid-filled porous solids and its application to overthrust faulting. *Geological Society of America Bulletin*, 70, 115–66.

- Key, R.M., Cotterill, F.P.D., Moore, A.E., 2015. The Zambezi River: An Archive of Tectonic Events Linked to the Amalgamation and Disruption of Gondwana and Subsequent Evolution of The African Plate. *South African Journal of Geology*, 118, 4, 425-438, <https://doi:10.2113/gssajg.118.4.425>
- King, L.H., MacLean, B., 1970. Pockmarks on the Scotian Shelf. *Bull. Geol. Soc. Am.*, 81 (1970), 3141-3148, <https://10.1130/0016-7606>
- Kolla, V., Eittreim, S., Sullivan, L., Kostecki, J.A., Burckle, L.H., 1980. Current-controlled, abyssal microtopography and sedimentation in Mozambique Basin, southwest Indian Ocean. *Marine Geology* 34, 171–206.
- Kolla, V., Kostecki, J. A., Henderson, L., Hess, L., 1991. Morphology and Quaternary Sedimentation of the Mozambique Fan and Environs, Southwestern Indian Ocean, in *Deep-Water Turbidite Systems* (ed. D.A.V. Stow), Blackwell Publishing Ltd., Oxford, UK. doi: 10.1002/9781444304473.ch36
- Krämer, K., Holler, P., Herbst, G., Bratek, A., Ahmerkamp, S., Neumann, A., Winter, C., 2017. Abrupt emergence of a large pockmark field in the German Bight, southeastern North Sea. *Scientific reports*, 7, 1, 1-8.
- Leinweber, V.T., Jokat, W., 2012. The Jurassic history of the Africa–Antarctica corridor—new constraints from magnetic data on the conjugate continental margins. *Tectonophysics* 530, 87-101.
- Mahanjane, E. S., Franke, D., 2014. The Rovuma Delta deep-water fold-and-thrust belt, offshore Mozambique. *Tectonophysics* 614, 91–99. <http://dx.doi.org/10.1016/j.tecto.2013.12.017>
- Mahanjane, E.S., Franke, D., Lutz, R., Winsemann, J., Ehrhardt, A., Berglar, K., Reichert, C., 2014. Maturity and petroleum systems modelling in the offshore Zambesi Delta depression and Angoche Basin, northern Mozambique, *J. Pet. Geol.*, 37(4), 329–348.
- Mahanjane, E.S., 2012. A geotectonic history of the northern Mozambique Basin including the Beira High – A contribution for the understanding of its development. *Marine and Petroleum Geology* 36, 1–12. <https://doi.org/10.1016/j.marpetgeo.2012.05.007>
- Marsset, T., Ruffine, L., Ker S., Cauquil E., Gay A., 2018. Types of fluid-related features controlled by sedimentary cycles and fault network in deepwater Nigeria. *Marine and Petroleum Geology*, 89, Part. 2, 330-349. <https://doi.org/10.1016/j.marpetgeo.2017.10.004>
- Marsset, T., Jouet, G., Courgeon, S., Jatiault, R., Deville, E., 2018. Map of the active fault system across the oceanic lithosphere of the Mozambique Channel, from the data of the

- PTOLEMEE (2014), PAMELA-MOZ02 (2014) and PAMELA-MOZ04 (2015) marine expeditions. SEANOE DOI10.17882/55634. <http://www.seanoe.org/data/00445/55634/>
- Masclé, J., Mary, F., Praeg, D., Brosolo, L., Camera, L., Ceramicola, S., Dupré, S., 2014. Distribution and geological control of mud volcanoes and other fluid/free gas seepage features in the Mediterranean Sea and nearby Gulf of Cadiz. *Geo-Mar. Lett.* 34, 89–110. <http://dx.doi.org/10.1007/s00367-014-0356-4>
- Migeon, S., Ceramicola, S., Praeg, D., Ducassou, E., Dano, A., Ketzer, J.M., Mary, F., Masclé, J., 2014. Post-failure processes on the continental slope of the central Nile Deep-sea fan: Interactions between fluid seepages, sediment deformation and sediment-wave construction. *Submarine mass movements and their consequences, Advances in natural and technological research* 37, Krastel, S. et al. (eds), 117– DOI10.1007/978-3-319-00972-8_11
- Miramontes, E., Penven, P., Fierens, R., Droz, L., Toucanne, S., Jorry, S., Jouet, G., Pastor, L., Silva Jacinto, R., Gaillot, A., Giraudeau, J., Raisson, F., 2019. The influence of bottom currents on the Zambezi Valley morphology (Mozambique Channel, SW Indian Ocean): In situ current observations and hydrodynamic modelling. *Marine Geology*, 410, 42–55. <https://doi.org/10.1016/j.margeo.2019.01.002>
- Moore, A.E, Cotterill, F.P.D., Main, M.P.L., Williams, H.B., 2007. The Zambezi River. In: A. Gupta 902 (Editor), *Large Rivers: Geomorphology and Management*. Wiley, Chichester, 311–331.
- Mueller, C.O., Jokat, W., Schreckenberger, B., 2016. The crustal structure of Beira High, central Mozambique—Combined investigation of wide-angle seismic and potential field data. *Tectonophysics* 683, 233–254.
- Mueller, C.O., Jokat, W., 2017. Geophysical evidence for the crustal and distribution of magmatism along the central coast of Mozambique. *Tectonophysics* 712–713, 684–703.
- Mueller, C. O.; Jokat, W., 2019. The initial Gondwana break-up: A synthesis based on new potential field data of the Africa-Antarctica Corridor. *Tectonophysics*, 750, 301–328.
- Naehr, T.H. Rodriguez, N.M., Bohrmann, G., Botz, R., 2000. Methane-derived authigenic carbonates associated with gas hydrate decomposition and fluid venting above the Blake Ridge Diapir. *Proceedings of the Ocean Drilling Program: Scientific Results* 164, 285–300. <https://DOI:10.2973/odp.proc.sr.164.228.2000>.
- O'Leary, M.H., 1988. *Carbon Isotopes in Photosynthesis*. *BioScience* 38, 5, 328–336. <https://doi:10.2307/1310735>

- Orphan, V.J., House, C.H., Hinrichs, K.U., McKeegan, K.D., DeLong, E.F., 2001. Methane-consuming archaea revealed by directly coupled isotopic and phylogenetic analysis. *Science* 293, 5529, 484-487.
- Peckmann, J., Reimer, A., Luth, U., Reitner, J., 2001. Methane-derived carbonates and authigenic pyrite from the northwestern Black Sea. *Marine Geology* 177(1-2), 129-150. [https://doi.org/10.1016/S0025-3227\(01\)00128-1](https://doi.org/10.1016/S0025-3227(01)00128-1)
- Peckmann, J., Thiel, V., 2004. Carbon cycling at ancient methane-seeps. *Chemical Geology* 205, 443– 467. <https://doi.org/10.1016/j.chemgeo.2003.12.025>
- Pillot, D., Deville, É., Prinzhofer, A., 2014. Identification and Quantification of Carbonate Species Using Rock-Eval Pyrolysis. *Oil & Gas Sciences and Technologies. Oil & Gas Science and Technology*, 69, 2, 341-349. <https://doi.org/10.2516/ogst/2012036>.
- Pierre, C., Blanc-Valleron, M.-M., Demange, J., Boudouma, O., Foucher, J.-P., Pape, T., Himmler, T., Fekete, N., Spiess, V., 2012. Authigenic carbonates from active methane seeps offshore southwest Africa. *Geo-Mar. Lett.* 32, 501–513.
- Pierre, C., Bayon, G., Blanc-Valleron, M.M., Mascle, J., Dupré, S., 2014. Authigenic carbonates related to active seepage of methane-rich hot brines at the Cheops mud volcano, Menes caldera (Nile deep-sea fan, eastern Mediterranean Sea). *Geo-Mar. Lett.* 34, 253–267. <http://dx.doi.org/10.1007/s00367-014-0362-6>.
- Pierre, C., Demange, J., Blanc-Valleron, M.M., Dupré, S., 2017. Authigenic carbonate mounds from active methane seeps on the southern Aquitaine Shelf (Bay of Biscay, France): Evidence for anaerobic oxidation of biogenic methane and submarine groundwater discharge during formation. *Continental Shelf Research* 133, 13–25. <http://dx.doi.org/10.1016/j.csr.2016.12.003>
- Ponte, J.-P., 2018. La marge africaine du Canal du Mozambique (le Système turbiditique du Zambèze) : une approche Source to Sink au Méso-Cénozoïque. PhD Thesis, Rennes 1 University, 351 p.
- Ponte, J.-P., Robin, C., Guillocheau, F., Popescu, S., Suc, J.-P., Dall'Asta, M., Melinte-Dobrinescu, M.C., Bubik, M., Dupont, G., Gaillot, J., 2019. The Zambezi delta (Mozambique channel, East Africa): High resolution dating combining bio-orbital and seismic stratigraphy to determine climate (palaeoprecipitation) and tectonic controls on a passive margin. *Marine and Petroleum Geology* 105, 293-312, <https://doi.org/10.1016/j.marpetgeo.2018.07.017>
- Praeg, D., Ketzer, J.M., Augustin, A.H., Migeon, S., Ceramicola, S., Dano, A., Ducassou, E., Dupré, S., Mascle, J., Rodrigues, L.F., 2014. Fluid Seepage in Relation to Seabed

- Deformation on the Central Nile Deep-Sea Fan, Part 2: Evidence from Multibeam and Sidescan Imagery Submarine Mass Movements and Their Consequences - Natural and Technological Hazards Research Volume 37, 141-150 S. Krastel, S. et al. (eds), Springer ISBN 9783319009711 http://dx.doi.org/10.1007/978-3-319-00972-8_13, Springer International
- Prinzhofer A., Deville E., 2013. Origins of hydrocarbon gas seeping out from offshore volcanoes in the Nile delta. *Tectonophysics* 591, 52–61. <https://doi.org/10.1016/j.tecto.2011.06.028>.
- Quartly, G.D., Srokosz, M.A., 2004. Eddies in the southern Mozambique Channel. *Deep Sea Research* 920 Part II: Topical Studies in Oceanography 51, 69–83. <https://doi.org/10.1016/j.dsr2.2003.03.001>
- Rabinowitz, P. D., Coffin, M., Falvey, D., 1983. The separation of Madagascar and Africa, *Science*, 220, 67–69.
- Reeves, C., 2014. The position of Madagascar within Gondwana and its movements during Gondwana dispersal, *J. Afr. Earth Sci.*, 94, 45–57.
- Riboulot, V., Thomas, Y., Berné, S., Jouet, G., Cattaneo, A., 2014. Control of Quaternary sea-level changes on gas seeps. *Geophysical Research Letters* 41, 14, 4970-4977. <https://doi.org/10.1002/2014GL060460>
- Rongemaille, E., Bayon, G., Pierre, C., Bollinger, C., Chu, N.C., Fouquet, Y., Riboulot, V., Voisset, M., 2011. Rare earth elements in cold seep carbonates from the Niger delta. *Chem. Geol.* 286, 196-206.
- Salman, G., Abdula, I., 1995. Development of the Mozambique and Ruvuma sedimentary basins, offshore Mozambique. *Sedimentary Geology*, 96, 1-2, 7-41.
- Schulz, H., Lückge, A., Emeis, K.-C., Mackensen, A., 2011. Variability of Holocene to Late Pleistocene Zambezi riverine sedimentation at the upper continental slope off Mozambique, 15°–21°S. *Marine Geology* 286, 21–34. <https://doi.org/10.1016/j.margeo.2011.05.003>
- Sultan, N., Cochonat, P., Canals, M., Cattaneo, A., Dennielou, B., Haflidason, H., Laberg, J.S., Long, D., Mienert, J., Trincardi, F., Urgeles, R., Vorren, T.O., Wilson, C., 2004a. Triggering mechanisms of slope instability processes and sediment failures on continental margins: a geotechnical approach. *Marine Geology* 213, 291-321. <http://dx.doi.org/10.1016/j.margeo.2004.10.011>
- Sultan, N., Cochonat, P., Foucher, J.P., Mienert, J., 2004b. Effect of gas hydrates melting on seafloor slope instability, *Mar. Geol.*, 213, 379–401.

- Thompson, J.O., Moulin, M., Aslanian, D., de Clarens, P. , Guillocheau, F., 2019. New starting point for the Indian Ocean : Second phase of breakup for Gondwana, 191, 26-56. <https://doi.org/10.1016/j.earscirev.2019.01.018>
- Urlaub, M., Talling, P. J., Zervos, A., Masson, D., 2015. What causes large submarine landslides on low gradient ($<2^\circ$) continental slope with slow (~ 0.15 m/kyr) sediment accumulation? J. Geophys. Res. 120, 6722–6739 .
- Walford, H.L., White, N.J., Sydow, J.C., 2005. Solid sediment load history of the Zambezi Delta. Earth and Planetary Science Letters, 238, 1-2, 49-63.
- Whiticar, M.J., 1999. Carbon and hydrogen isotope systematics of bacterial formation and oxidation of methane. Chemical Geology 161. 291–314.
- Wiles E., Green A.N., Watkeys M.K., Jokat W., 2017a; Zambezi continental margin: compartmentalized sediment transfer routes to the abyssal Mozambique Channel. Mar Geophys Res. <https://doi.10.1007/s11001-016-9301-4>
- Wiles, E., Green, A.N., Watkeys, M., Jokat, W., 2017b. The Zambezi Channel: A new perspective on submarine channel evolution at low latitudes. Geomorphology, 121–132. 955. <https://doi.org/10.1016/j.geomorph.2017.02.014>
- Yoshinaga, M.Y., Holler, T., Goldhammer, T., Wegener, G., Pohlman, J.W., Brunner, B., Kuypers, M.M., Hinrichs, K-U., Elvert, M., 2014. Carbon isotope equilibration during sulphate-limited anaerobic oxidation of methane. Nature Geosciences 7, 190-194. <https://doi:10.1038/ngeo2069>.

FIGURES CAPTION

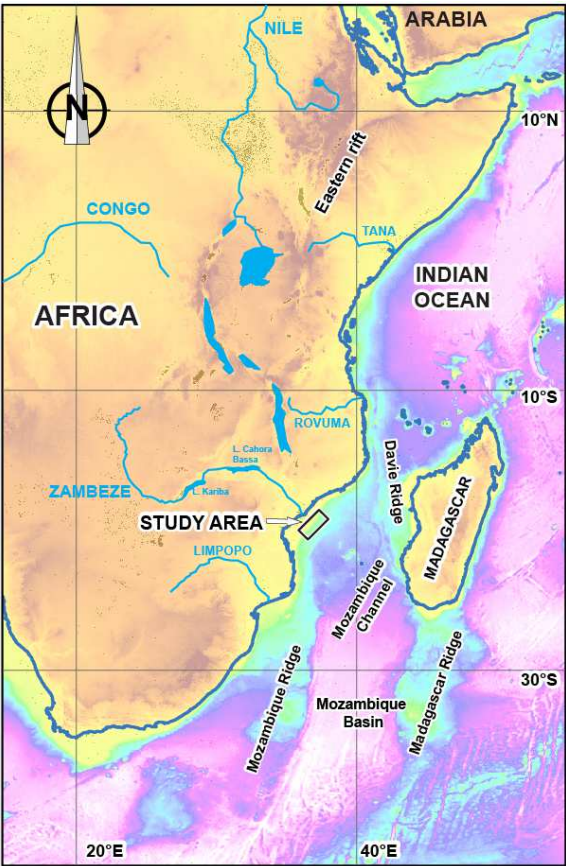


Figure 1. Location of the study area along the East African coast.

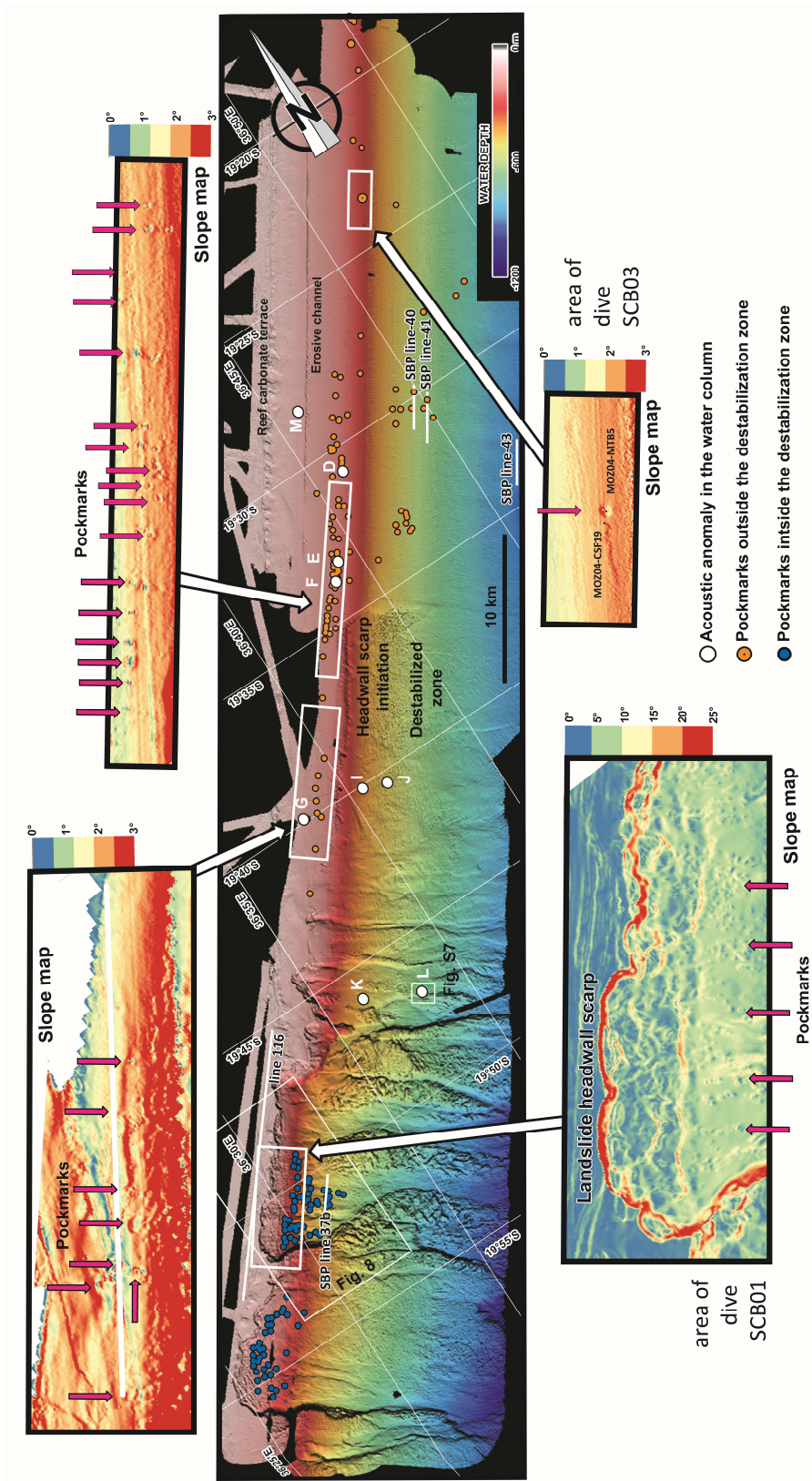
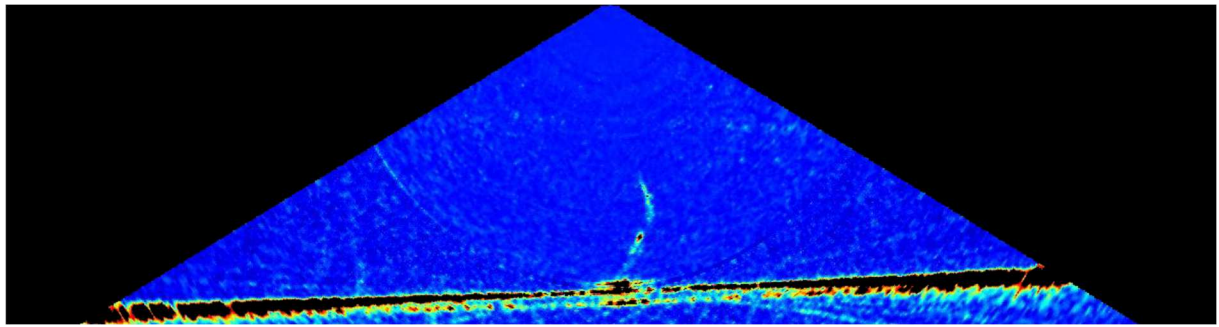
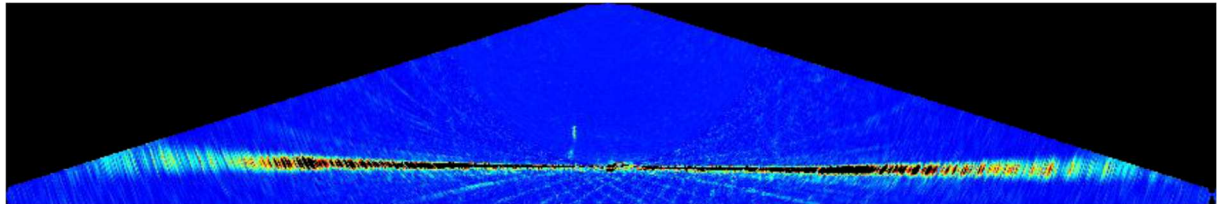


Figure 2. Location of the pockmarks and water column acoustic anomalies in the detailed study area (red arrows indicate the pockmark locations on slope maps; letters refer to sites where acoustic anomalies interpreted as free gas seepages have been detected in the water column).

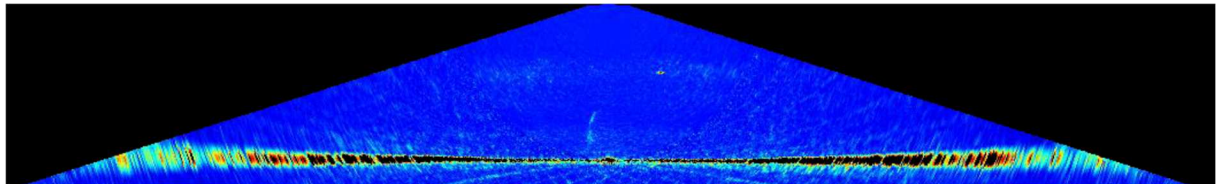
768



769



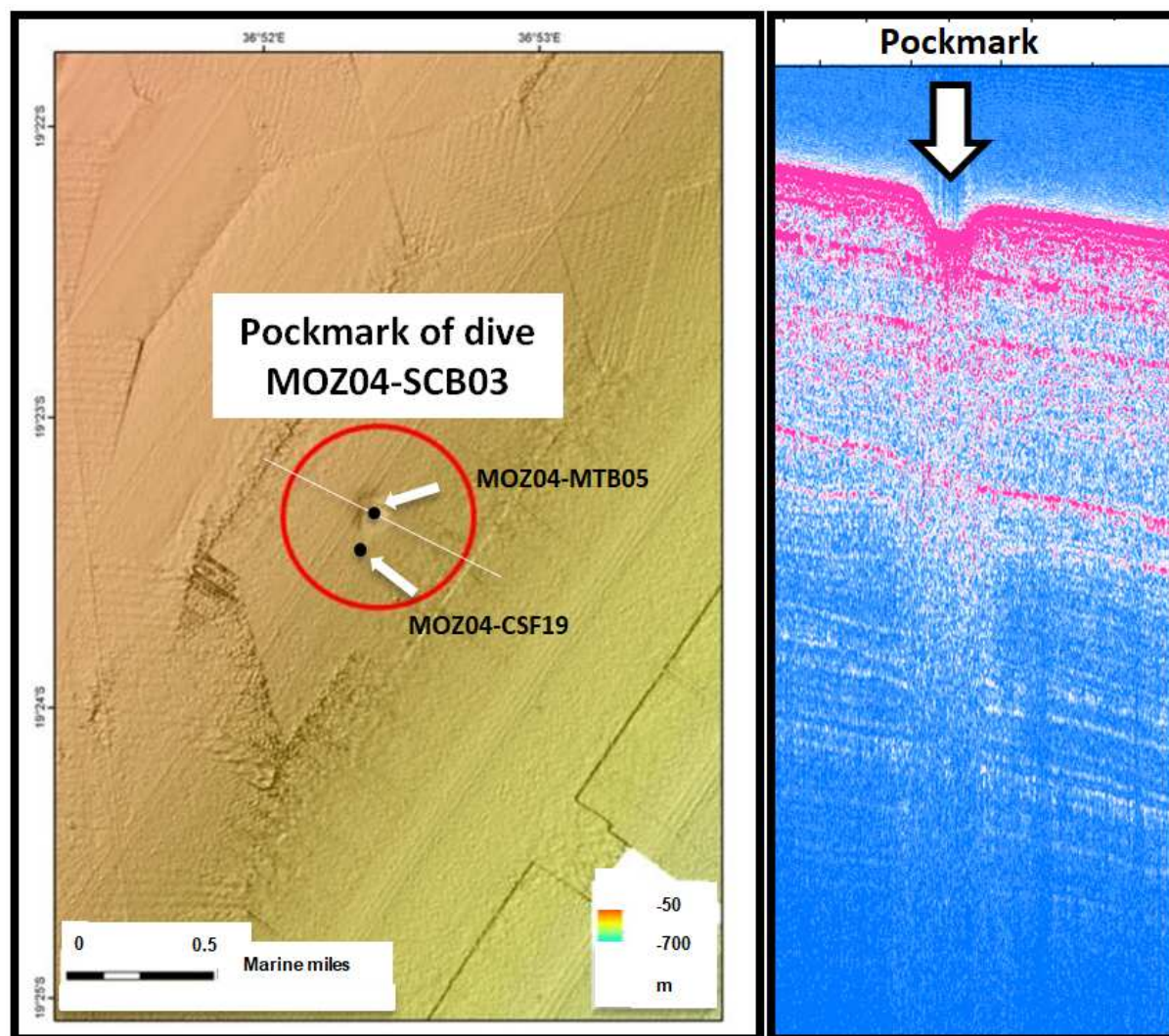
770



771

772 **Figure 3.** Examples of multibeam polar echograms of the water column with acoustic
 773 anomalies interpreted as fluid seepages associated with bubble fluxes corresponding to sites
 774 G. (top image), I (middle image) and J (bottom image). See figure 2 for locations.

775

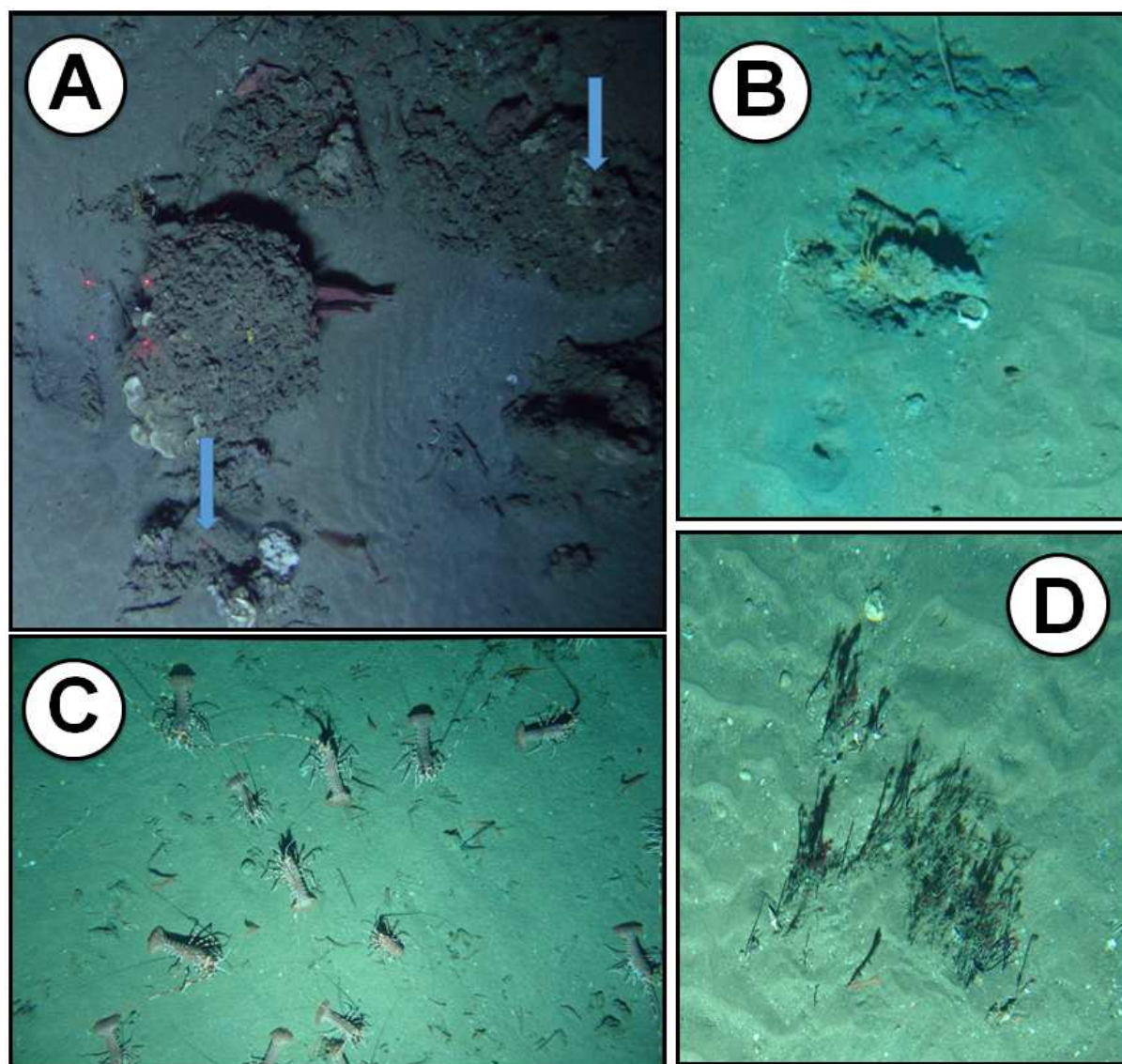


776

777

778 **Figure 4.** The pockmark of SCAMPI dive MOZ04-SCB03 (location in Fig. 2). Note the
 779 seismic anomalies on the SBP profile crossing this feature.

780



781

782

783 **Figure 5.** **A.** Authigenic carbonate crust in the pockmark of dive MOZ04-SCB03 (location in
784 Fig. 2), the two arrows indicate places where turbulences associated with fluid seepages have
785 been observed. **B.** Punctual seepages associated with expelled reduced sediments. **C.** Colony
786 of lobsters. **D.** Tubeworms (Siboglinidae) characteristic of methane seepages.



Figure 6. Photo of a carbonate conduit recovered in multitube sampler (MOZ04-MTB5; location in Fig. 2).

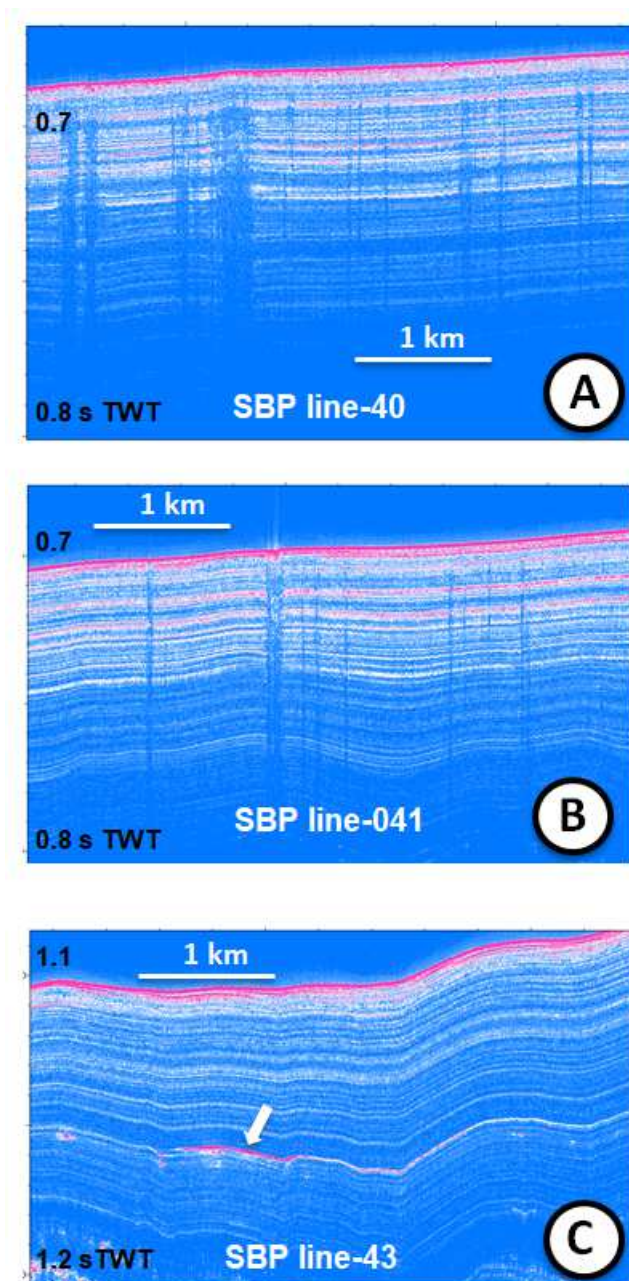


Figure 7. **A** and **B.** Examples of SBP lines acquired in the slope north-east of the slope destabilization zone showing vertical seismic anomalies interpreted as gas escape pathways. **C.** Example of SBP line showing an amplitude anomaly (white arrow) in a stratigraphic layer which is interpreted as a possible free gas occurrence (location of the SBP lines in Fig. 2).

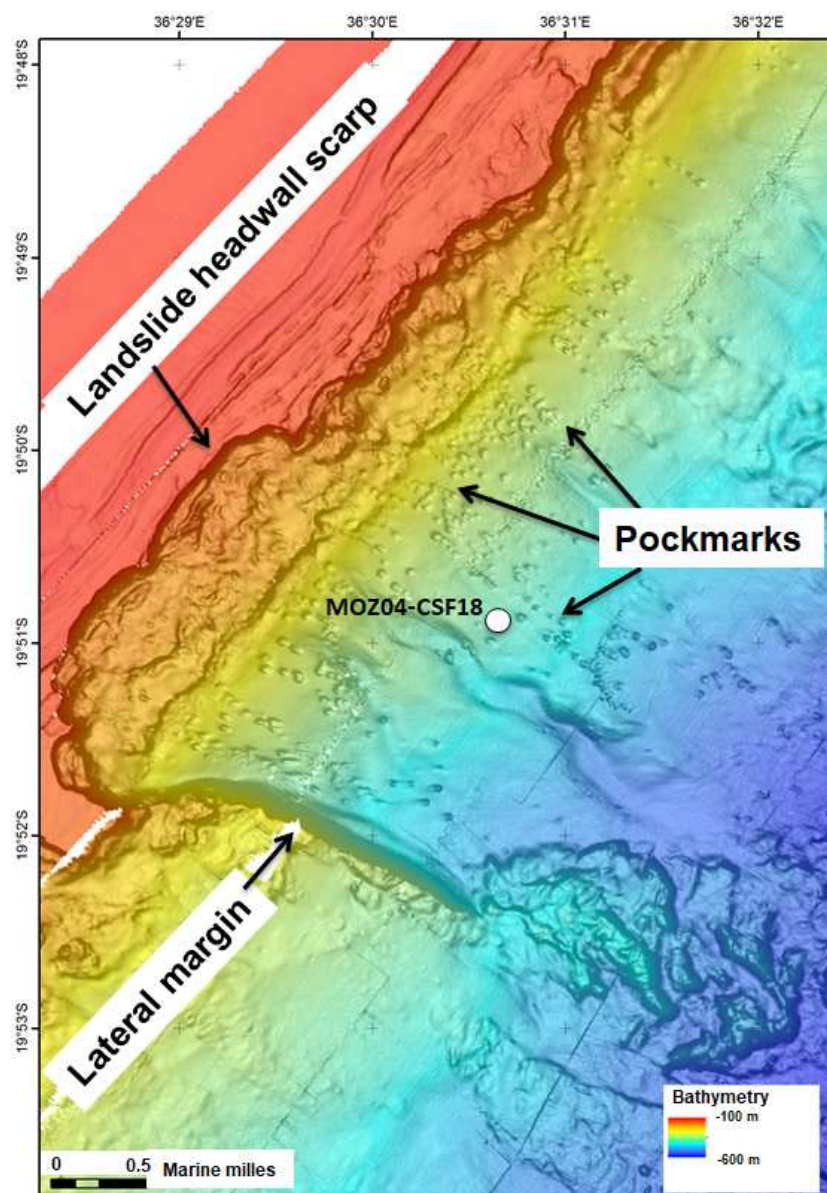
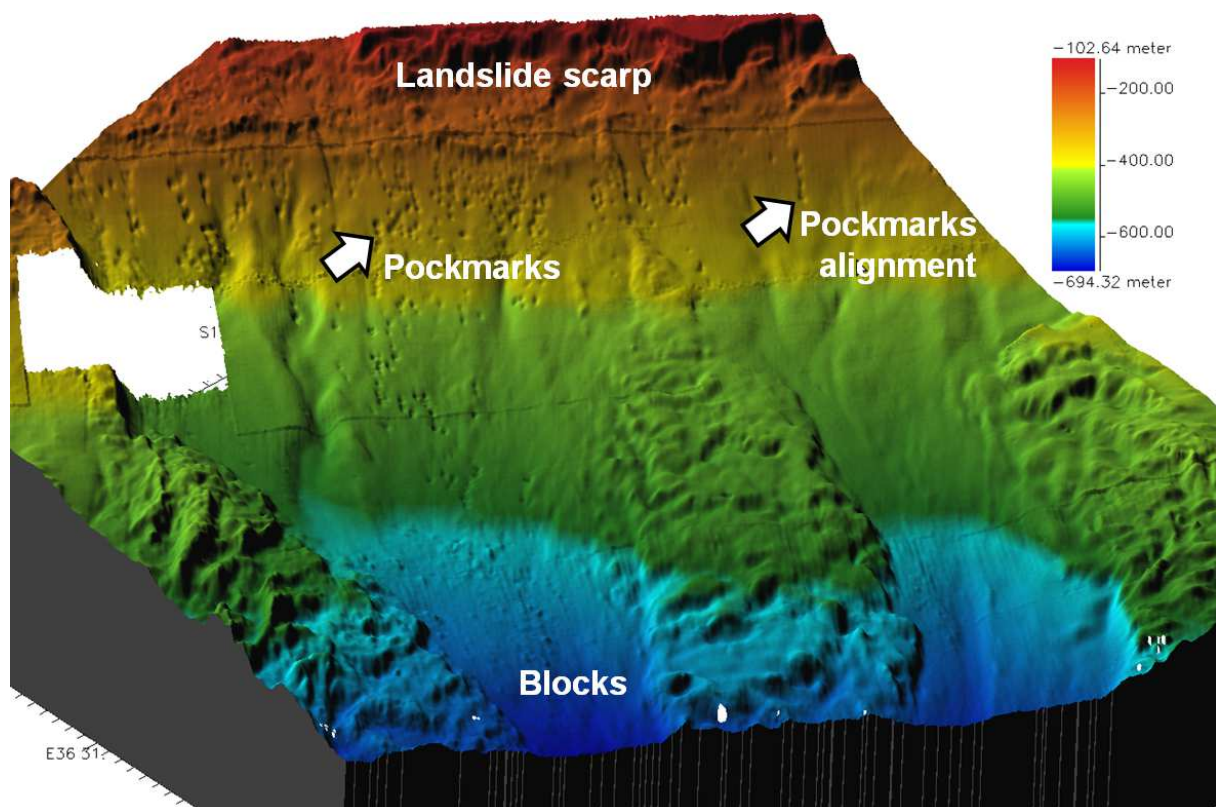


Figure 8. Detailed bathymetric map showing the distribution of the pockmarks in the center of the slope destabilization zone.

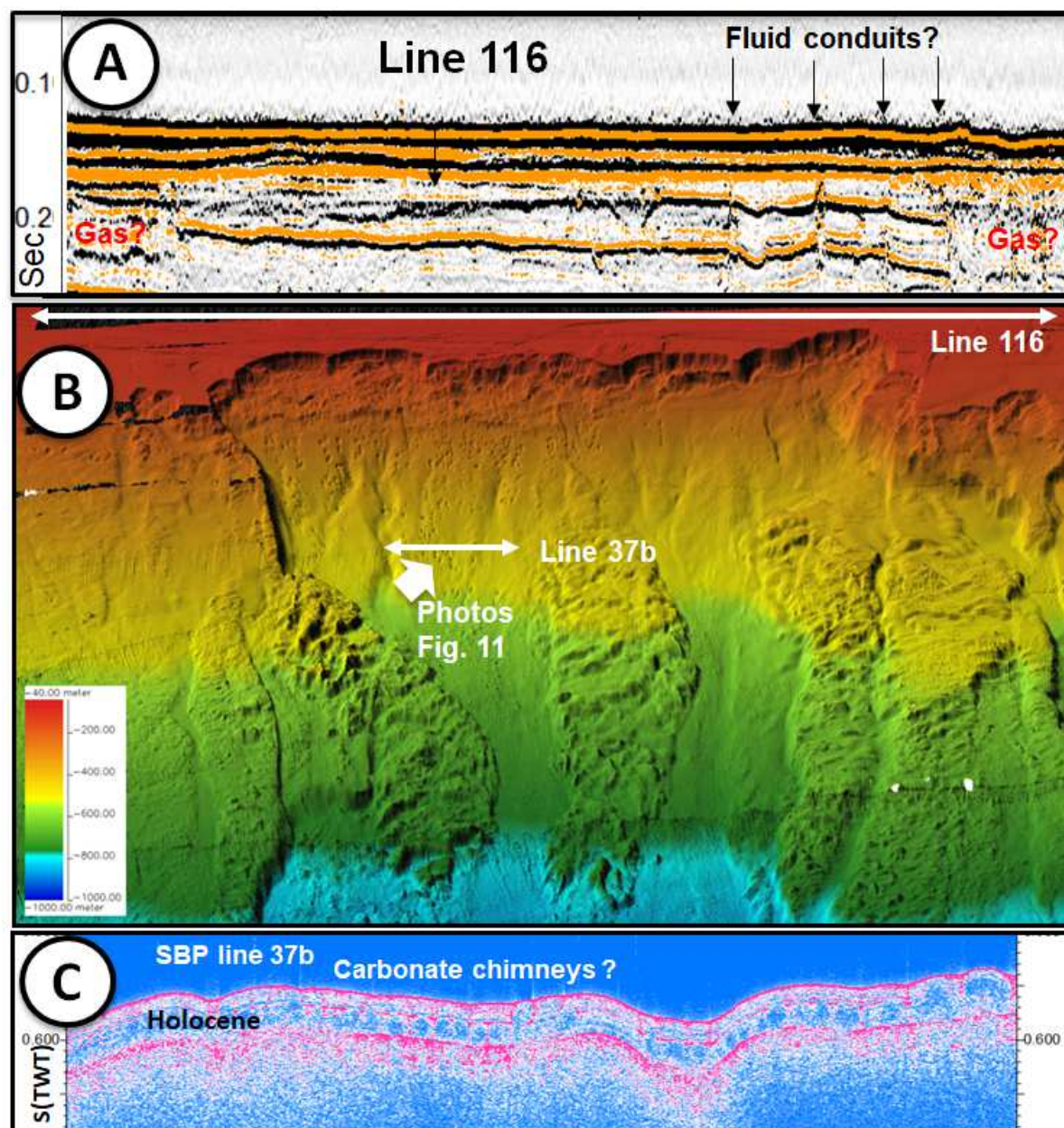
803



804

805 **Figure 9.** Block-diagram illustrating the location of the pockmarks of the zone of slope
 806 destabilization. Note the alignment of some of the pockmarks (vertical exaggeration x3).

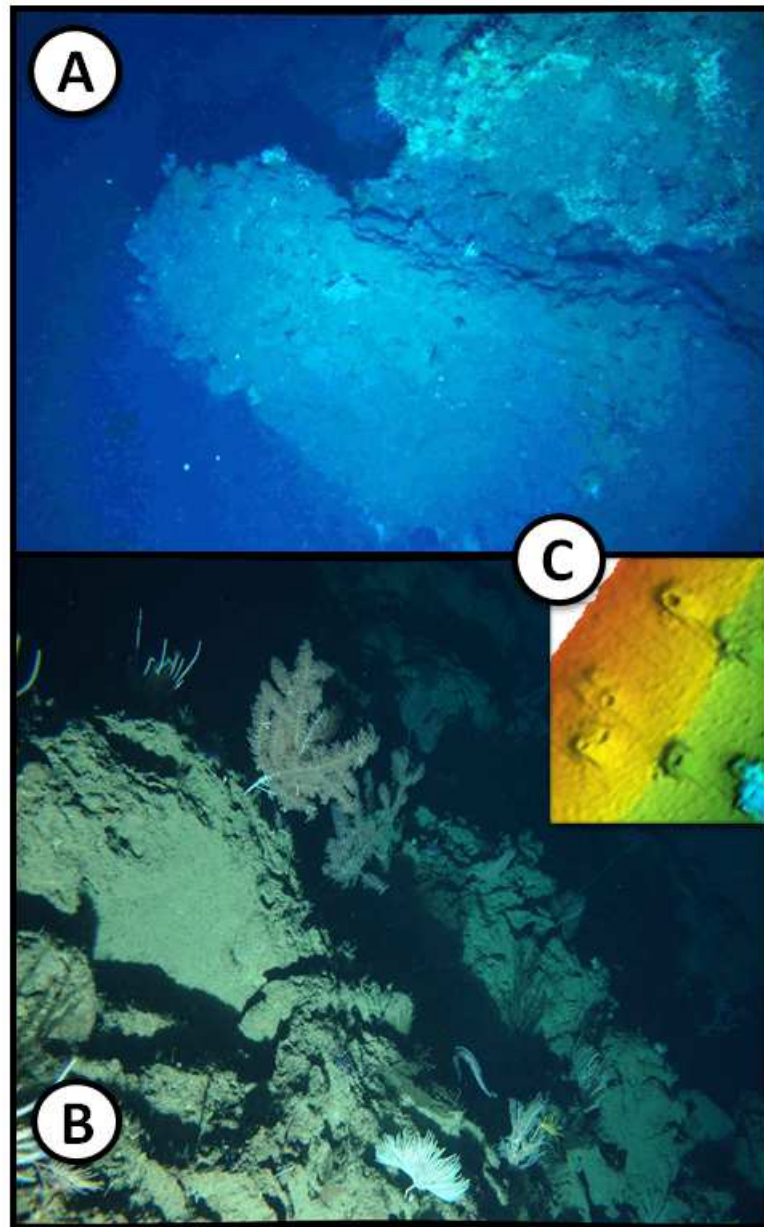
807



808

Figure 10. –A. High Resolution seismic line upstream of the destabilization area. Along this line some vertical seismic structures are interpreted as probable fluid conduits and, locally, zones of low amplitude chaotic seismic facies with acoustic mask are possibly related to the presence of free gas within the sediments. B. A perspective view of the center of the destabilization zone showing the distribution of the pockmarks and the location of seismic reflection line 116 (Fig. 10A) and the SBP line 37b (Fig. 10C). Note also the presence of gullies without any apparent correlation with the pockmarks alignments. C. SBP profile showing vertical seismic structures below the pockmarks which are possibly related to carbonate fluid chimneys.

818

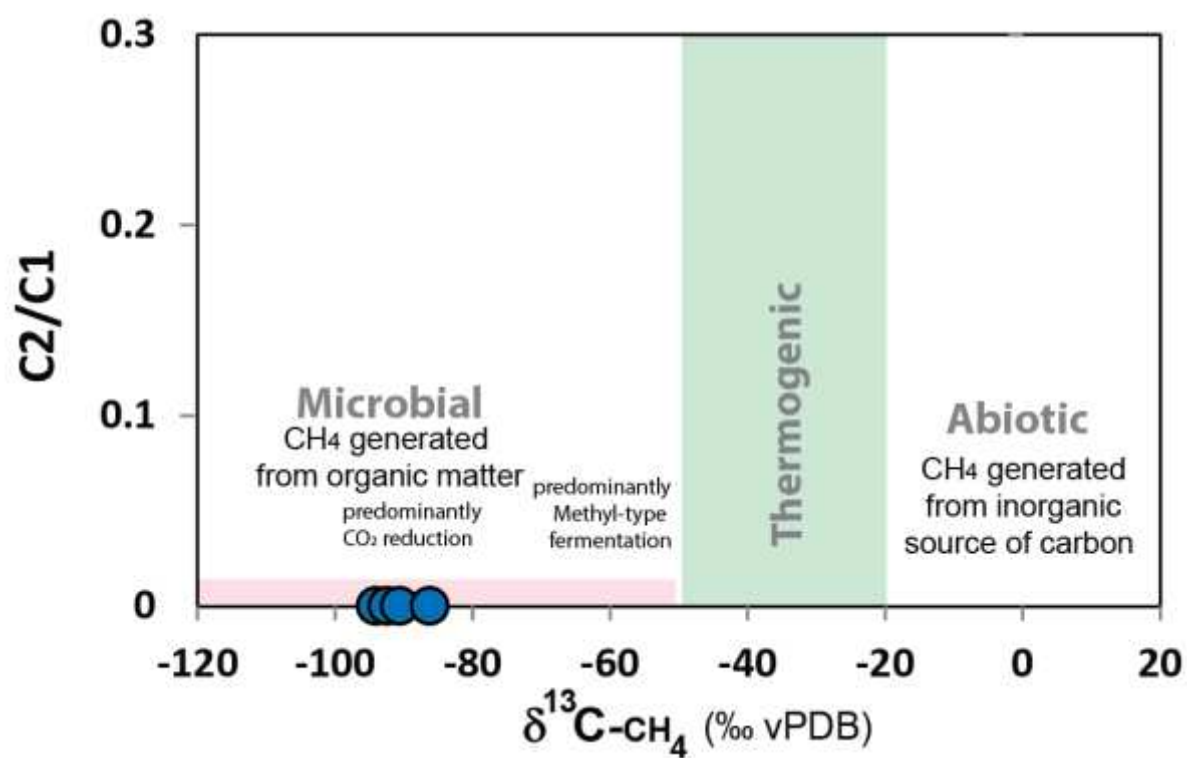


819

820

821 **Figure 11.** – **A.** Picture of the top of a carbonate chimney observed in a pockmark of the
 822 center of the slope destabilization zone (this structure is about 4 m in diameter and 8 m high;
 823 location Fig. 10). **B.** A side of one of the carbonate chimney covered by gorgones. **C.** Detailed
 824 bathymetric map showing the internal geometry of the pockmarks depressions inside the
 825 destabilization zone with carbonate chimneys in the center of the comet-shaped depressions.

826

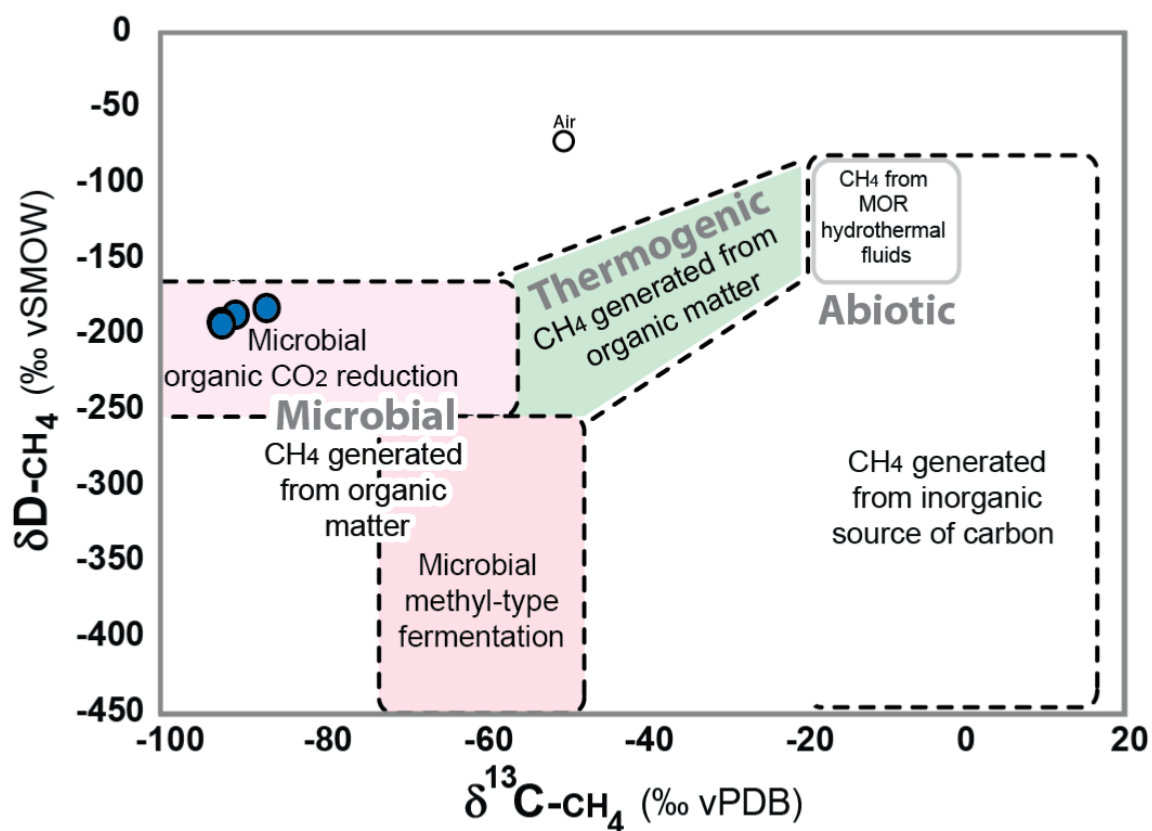


827

828 **Figure 12.** Diagram δ¹³C of methane versus C₂/C₁ for gases collected in the study area.

829

830



831

832 **Figure 13.** Diagram $\delta^{13}C$ of methane versus δD of methane for gases collected in the study
 833 area.

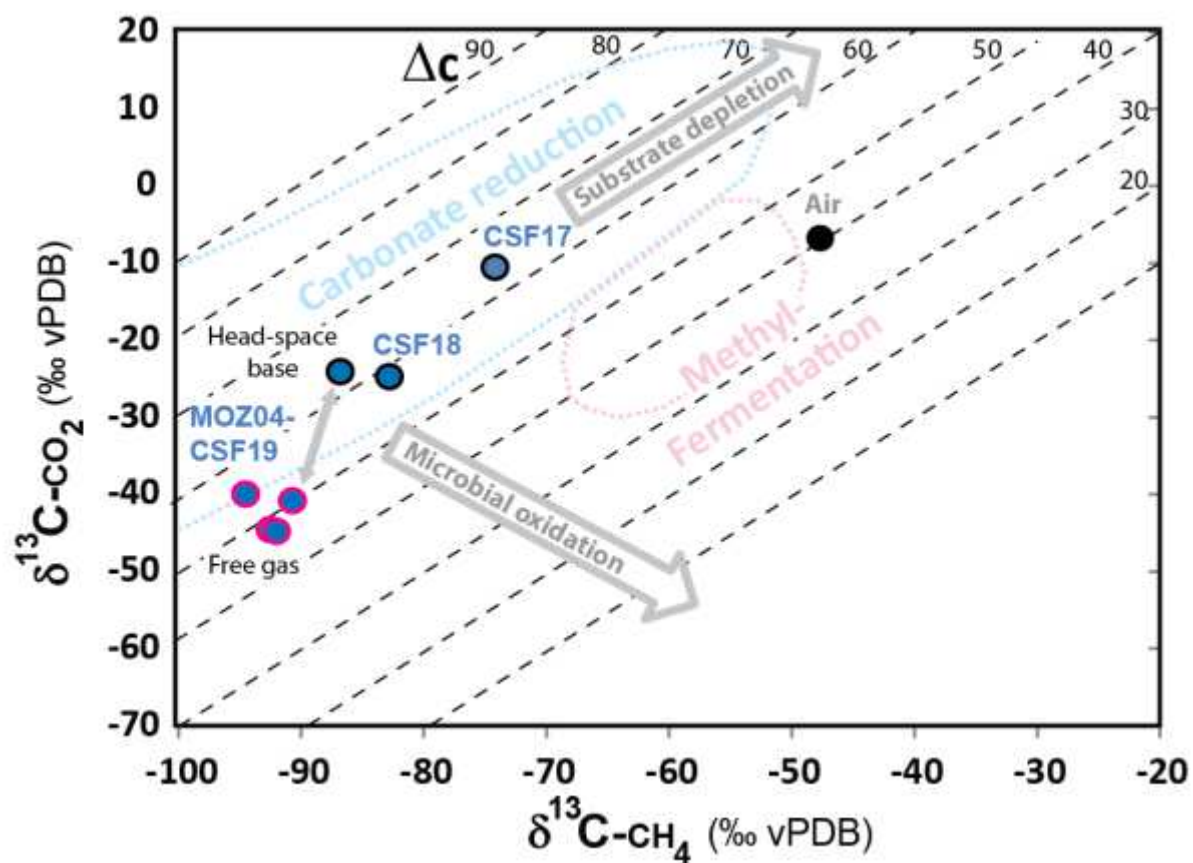
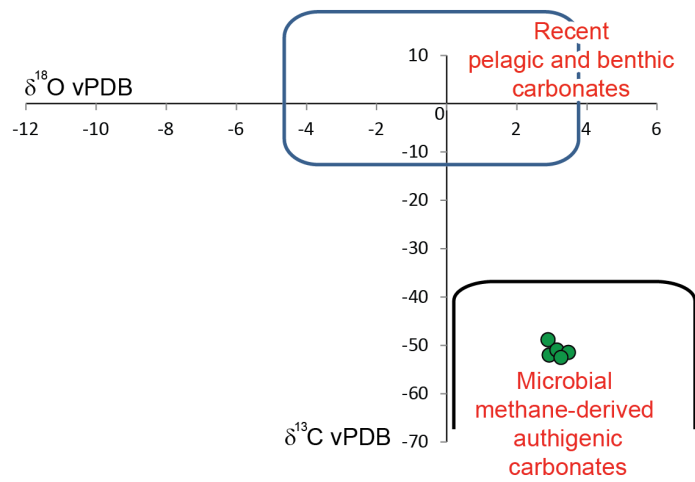


Figure 14. Diagram $\delta^{13}\text{C}$ of methane versus $\delta^{13}\text{C}$ of CO_2 for gases collected in the study area (domains after Whiticar, 1999).

838



839

840

841 **Figure 15.** Isotopic composition of the sampled carbonates in core MOZ04-MTB5 (location
842 in Figs. 2 and 4).

843

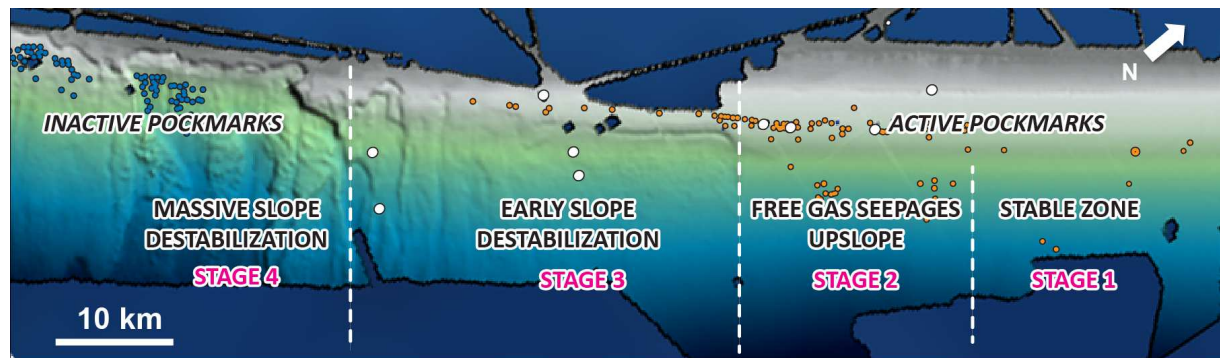


Figure 16. Relationship between fluid seepages and slope destabilization.

847

Sample type	Sample	CH ₄ (%)	CO ₂ (%)	CH ₄ /CO ₂	Air (%)
Free gas	MOZ4-CSF19-B(A)	96.62	3.38	28.63	62.74
	MOZ4-CSF19-B(B)	96.10	3.90	24.63	44.80
	MOZ4-CSF19-B(C)	96.26	3.74	25.72	54.70
	MOZ4-CSF19-B(D)	96.24	3.76	25.57	15.32
	MOZ4-CSF19-B(E)	95.72	4.28	22.38	61.82
	MOZ4-CSF19-B(I)	96.43	3.57	27.02	78.10

848 **Table 1.** Composition of the free gas sample on core MOZ4-CSF19.

Type of sample	Sample	$\delta^{13}\text{C-CH}_4$ (‰)	$\delta^{13}\text{C-CO}_2$ (‰)	$\delta\text{D-CH}_4$ (‰)	$\Delta\text{C}_{\text{CH}_4-\text{CO}_2}$
Free gas	MOZ4-CSF19-B(A)	-90.5	-40.5	-175.4	50.0
in liner	MOZ4-CSF19-B(B)	-92.4	-44.3	-180.5	48.1
	MOZ4-CSF19-B(C)	-92.2	-44.5	-182.2	47.7
Adsorbed gas at core base					
32.5m	MOZ4 CS17 (OG)	-74.1	-10.2	-178.7	63.9
9.5 m	MOZ4 CSF18 (OG)	-82.7	-24.4		58.3
9.5 m	MOZ4 CSF19 (OG)	-86.7	-23.8	-170.5	62.9

Table 2. Isotopic composition and isotopic carbon separation values between CH₄ and CO₂ of the gas samples collected on cores MOZ4-CSF17, MOZ4-CSF18 and MOZ4-CSF19.

	$\delta^{18}\text{O}$ (‰)	$\delta^{13}\text{C}$ (‰)
	V-PDB	V-PDB
MOZ4-MTB5-A	2.89	-48.87
MOZ4-MTB5-B	2.93	-52.02
MOZ4-MTB5-C	3.15	-51.00
MOZ4-MTB5-D	3.47	-51.48
MOZ4-MTB5-E	3.26	-52.50

851 **Table 3.** Isotopic composition of the carbonate samples collected on core MOZ4-MTB5.

852

853